Signal Design and Processing Techniques for WSR-88D Ambiguity Resolution

Further Investigation

National Severe Storms Laboratory Report

prepared by: M. Sachidananda
with contributions by: D. S. Zrnić and R. J. Doviak

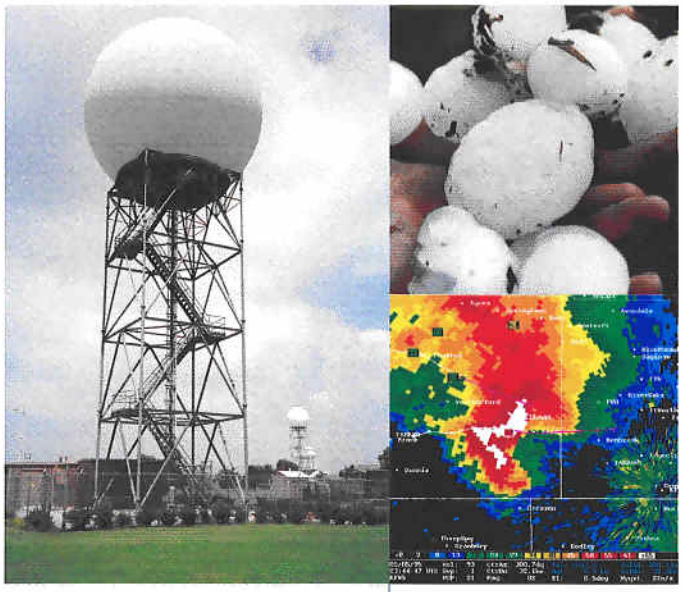

Part 5
October 2001

National Oceanic and Atmospheric Administration
National Severe Storms Laboratory
Norman, Oklahoma 73069

SIGNAL DESIGN AND PROCESSING TECHNIQUES FOR WSR-88D AMBIGUITY RESOLUTION

PART – 5: Further Investigation

National Severe Storms Laboratory Report

prepared by: M. Sachidananda,
with contributions by: D.S. Zrnic and R.J. Doviak

October 2001

NOAA, National Severe Storms Laboratory
1313 Halley Circle, Norman, Oklahoma 73069

SIGNAL DESIGN AND PROCESSING TECHNIQUES FOR WSR-88D AMBIGUITY RESOLUTION
Part-4: Some Investigations.

Contents

ooo000ooo

SIGNAL DESIGN AND PROCESSING TECHNIQUES FOR WSR-88D AMBIGUITY RESOLUTION

Part–5: Further Investigation

1. Introduction

The Radar Operations Center (ROC) of the National Weather Service (NWS) has funded the National Severe Storms Laboratory (NSSL) to address the mitigation of range and velocity ambiguities in the WSR-88D. This is the fifth report in the series that deals with range-velocity ambiguity resolution in the WSR-88D. The first two reports mainly dealt with the uniform PRT transmission and phase coding techniques to resolve the range ambiguity. Although the phase coding techniques do not directly address the velocity ambiguity problem, their capability to separate overlaid echoes allows the use of shorter PRTs which, in turn, diminishes the occurrence of ambiguous velocities. In the third report, we considered the staggered PRT technique and its variants. A significant outcome of the work is a new staggered PRT sequence processing technique in the spectral domain with significantly improved spectral moment estimates, and a clutter filtering technique that recovers velocity information over the entire extended unambiguous velocity interval without any drop-out regions. The only assumption made in the algorithm is that there are no overlaid signals. This necessarily restricts the selection of T_1 (the short PRT segment) to be sufficiently large for a given elevation so that the probability of overlay is small.

After the third report was submitted in July 1999, some more ideas were explored in an effort to further improve the staggered PRT scheme. Specifically, we tried to reduce the velocity estimate errors by optimizing the window weights. We also examined the possibility of extending the unambiguous range from r_{a1} to r_{a2}, by resolving one-overlay situation. The one-overlay situation is one in which only the short PRT can generate

overlaid echoes in the long PRT interval. Exhaustive simulations were carried out to evaluate the performance of the staggered PRT decoding scheme, and determine the limits of spectral moment recovery within acceptable range under various conditions. This information is very useful in developing a data censoring strategy to discard or flag the bad data. The results from all these studies are in Report 4.

There are several points that were left out during the course of the study of the range-velocity ambiguity problem in the WSR-88D. Some of these are addressed in this fifth report. In the SZ phase coding technique, suggested for low elevation angle scans of the WSR-88D radar, an alternative to the magnitude deconvolution, called the substitution method, is proposed by Frush (1999). A comparative study was carried out to evaluate its performance vis-à-vis the magnitude deconvolution proposed by Sachidananda and Zrnic (1999). These results are discussed in Section 2 of this report. Apart from the Section 2, which pertains to the SZ coding technique, the rest of the report is concerned with the staggered PRT technique.

During one of the review meetings concerning the range-velocity ambiguity work, Jim Evans (2001) suggested to examine the possibility of estimating the aliased velocity from the autocorrelation R_1 and de-alias it using R_2, for the staggered PRT technique. On examination, it is found that this indeed is possible in the absence of clutter, and the estimate variance is much lower than using other methods. We have evaluated this technique using simulation and compared it with other methods. The results are presented in Section 3.

In the course of examination of the suggested spectral domain ground clutter filtering technique for the staggered PRT sequence, the theoretical analysis showed a possibility of exact complex reconstruction of the lost signal components. The theory and conclusions arrived at after testing the procedure using simulations is presented in Section 4.

A fifth section deals with the recovery of spectral moments of weather signals that have very narrow spectrum widths overlapping a very strong ground clutter return. Most of our results presented in Report 3 and 4 dealt with weather signals of width 4 m s^{-1}. The specific case of a very narrow width signal (w<1 m s^{-1}) overlapping the clutter requires a

window function with much lower side lobes than that used for larger widths. This is discussed in Section 5.

A new Sigmet processor has been connected (in a passive mode) to the WSR-88D research radar at NSSL. Thus we were able to record some time series data using uniform PRT transmission. Although the staggered PRT is not programmed in yet, we can derive a staggered PRT time series from the uniform PRT sequence by dropping appropriate samples. Further, the uniform sample set can be processed by standard algorithms and the spectral moments compared with those of the staggered set. A comparative study of different data sets has been carried out and some statistics of the standard error has also been generated using the actual radar data. All these results are presented in Section 6.

Finally, there were some lacunae in the suggested vcp-11 scan strategy for the WSR-88D in Report 4. These recommendations are reviewed and revised tables with additional inputs are given in the last section.

2. Magnitude deconvolution and the substitution in SZ-1: a comparison of performance

Sachidananda et al. (1997) proposed the SZ-1 algorithm for retrieving the mean velocity and spectrum width of the weaker of the two overlaid signals from the SZ(8/64) phase encoded sequence of returned echoes. The algorithm uses recohering and magnitude deconvolution. First the stronger signal is removed by a spectral domain notch filter of width equal to ¾ of the total number of spectral coefficients, centered on the stronger signal mean velocity. The remaining ¼ of the spectrum contains two replicas of the weaker signal, which when recohered produce the original signal and symmetrically spaced side bands. The mean velocity, obtained from this time series, is a very good estimate in spite of the side bands presence. There is no bias in the velocity estimate because side bands are symmetric. Nonetheless, the spectrum width is affected by the side bands. To reincorporate the power from the side bands into the main spectral lobe, a magnitude domain deconvolution is carried out before the spectrum width is computed.

Frush (1999) proposed an alternative, called the substitution method. In it, the phase difference between the two replicas available in the remaining ¼ of the spectrum (after notch filtering) is used to reconstruct the deleted replicas of the weaker signal

spectral coefficients. Because the spectrum is a convolution of the signal spectrum with the code spectrum, the sequence of the phase shifts for the replicas progress in predetermined increments, each of which is unique. For the SZ(8/64) coded time series these unique increments can be derived from the code spectrum. The spectrum thus reconstructed by substitution, is transformed to the time domain and recohered to reconstruct the original signal without any side bands. Therefore, both the mean velocity and spectrum width can be computed from it.

The deconvolution operation is a matrix multiplication (i.e., pre-multiply the spectrum matrix with the deconvolution matrix). We also need to compute the autocorrelation $R(1)$ twice, once before the deconvolution to obtain the mean velocity and again after the deconvolution to obtain the spectrum width. This repetition is because the deconvolution procedure increases the estimate variance whenever the spectrum is not "narrow" (see Sachidananda et al. 1998), hence to get a better mean velocity estimate it is necessary to compute the velocity before the deconvolution. The substitution method requires computation of phase differences, comparisons with the code spectrum sequence of phase differences to determine the match, then shift the phase of the spectral replicas by the successive phase difference sequence, and substitution of these replicas in the place where the notch filter was applied. The rest of the computations are the same for the two algorithms.

Both these procedures are developed based on the assumption of a "narrow" spectrum as defined by Sachidananda et al. (1998). If the spectrum is "narrow" both methods are exact and give the same results. The difference in the performance in terms of the estimate variances arises because the "narrow" spectra criterion is not exactly satisfied in actual weather signals, and the noise is always present along with the signal. If the spectral spread is more than $1/8^{th}$ of the Nyquist interval, the replicas in the SZ coded signal spectrum overlap, and the reconstruction is not exact. It is this aspect that is compared here using simulation procedure to generate the statistics of velocity and spectrum width recovery. The SZ-1 decoding algorithm is reproduced here from Sachidananda et al. 1998) to conveniently compare the two methods. The details of the substitution procedure used in this simulation study are also presented before the results are discussed.

2.1 The SZ-1 decoding algorithm

This algorithm was developed for SZ(n/64) coded transmission in the short PRT mode (i.e., the shorter of two PRTs used in the successive scans at the lowest two elevations). The step by step procedure follows (for details of the algorithm and description of math symbols, see Sachidananda et al. (1998), depending on the context = is often used as in a programming language to indicate substitution of a variable into a memory register).

<<< **START** of algorithm (*stand alone mode; **does not** use long PRT data*)

1. Input raw time series E_{1k} ; k=1,2, ... M.
   - The phase switching sequence ψ_k ; SZ(n/M) code.
2. Cohere the 1st trip signal.
   - $E_1 = E_{1k} \exp\{-j\psi_k\}$.
   - 1st trip is coherent; 2nd trip is phase coded by a sequence
     $\varphi_k = n\pi k^2/M$; k=0,1,2,.... M-1.
3. Multiply by von Hann window weights, h_k.
   - $E_1 = E_1 h_k$.
4. Filter the ground clutter.
   - E_1 = GCF(E_1).
5. Cohere the second trip.
   - $E_2 = E_1 \exp\{-j\varphi_k\}$.
6. Autocovariance process E_1 and E_2 to get $\hat{p}_1,\hat{v}_1,\hat{w}_1,\hat{w}_1'$ and $\hat{p}_2,\hat{v}_2,\hat{w}_2,\hat{w}_2'$
   (for the computation of $\hat{w}_1',\hat{w}_2'$ use Eq. 6.27 of Doviak and Zrnic, 1993, and for the computation of $\hat{w}_1,\hat{w}_2$ use Eq. 6.32 of Doviak and Zrnic, 1993).
7. Compute $\hat{w}_1'/\hat{w}_2'$ ratio.
   - if $\hat{w}_1'/\hat{w}_2' > 1$, trip=2, second trip is stronger - process E_2.
   - if $\hat{w}_1'/\hat{w}_2' < 1$, trip=1, first trip is stronger - process E_1.

8. If trip=2, interchange E_1 & E_2, and all the parameters in step number 6.

- with this interchange, E_1 is the time series with stronger signal coherent.
- we need to recover $\hat{p}_2$,$\hat{v}_2$ and $\hat{w}_2$ of the weaker signal.

[Note: The processing steps 9 to 17 are the same for the two cases in step 7 with E_1 replaced by E_2. This is accomplished by step 8, and the trip numbers are restored in the step 18.]

9. Compute spectrum of E_1.

- $S_1' = \text{DFT}\ [\ E_1\ ]$.

10. Notch ($n_w M$) coefficients centered on $\hat{v}_1$ to get S_1 from S_1'.

Note: (a) n_w is not to exceed the maximum permissible value, (1-2n/M).

(b) for SZ(8/64) & SZ(12/64) optimum PNF center location to be computed if trip=1 (i.e. 1st trip stronger) and GCF is applied.

11. Compute the mean power p from the remaining coefficients.

Multiply p by $1/(1-n_w)$ to get mean power estimate $\hat{p}_2$.

12. Compute power ratio $pr = 10 \log_{10}(\hat{p}_1/\hat{p}_2)$ dB.

13. If pr< 25 dB, correct error in $\hat{p}_1$ estimate.

- $\hat{p}_1' = \hat{p}_1 - \hat{p}_2$.
- compute corrected power ratio $\hat{p}r = \hat{p}_1'/\hat{p}_1$.

14. Cohere the weaker signal in S_1.

- $e_1 = \text{IDFT}\ [\ S_1\ ]$
- if trip = 1, $e_2 = e_1 \exp\{-j\varphi_k\ \}$.
- if trip = 2, $e_2 = e_1 \exp\{\ j\varphi_k\ \}$.

15. Compute autocorrelation $R(1)$ for e_2, and compute mean velocity, $\hat{v}_2$.

16. Magnitude deconvolution. (for SZ(8/64) and SZ(16/64) only)

- compute magnitude spectrum, $s_2' = |\ \text{DFT}(e_2)\ |$.
- multiply by the deconvolution matrix, $s_2 = D\ s_2'$.

[The deconvolution matrix, D, is a part of the program. D is pre-computed and supplied to the algorithm, or stored as a

part of the program.]

17. Compute autocorrelation $R(1)$ for s_2, and compute width, $\hat{w}_2$.

18. If trip = 2, interchange parameters ($\hat{p}_1$,$\hat{v}_1$,$\hat{w}_1$) and ($\hat{p}_2$,$\hat{v}_2$,$\hat{w}_2$).

19. Output the 1st and 2nd trip parameters and go to the next sequence.

<<<----------**END** of algorithm

Modifications of the SZ-1 algorithm required by the substitution method.

To use the **substitution** instead of **magnitude deconvolution** in the SZ-1 algorithm, the following steps need to be modified. The steps #1 to #13 are the same. The steps #14 to #17 have to be replaced by the following steps(#14 to #16):

---

14. Reconstruct complete S_1 using substitution (for SZ(8/64) and SZ(16/64) only; details of this step for SZ(8/64) are given in section 2.2).

15. Cohere the weaker signal in S_1.

- e_1 = IDFT [S_1]
- if trip = 1, $e_2 = e_1 \exp\{-j\varphi_k\}$.
- if trip = 2, $e_2 = e_1 \exp\{j\varphi_k\}$.

[Note: This entire step 15 can be replaced by complex deconvolution in the frequency domain, because the corresponding convolution matrix is not singular if the filter function is deleted.]

16. Compute autocorrelation $R(1)$ for e_2, and compute mean velocity, $\hat{v}_2$, and width, $\hat{w}_2$.

The substitution method is based on the observation that if the signal spectrum is "narrow", the spectral replicas of signal modulated with the SZ(8/64) code differ in phase by the amount equal to the phase differences of the code spectral lines. This follows

from the nature of the code, because the eight replicas are obtained from the convolution of the original signal spectrum and the code spectrum. The spectrum of the modulation code $exp(jk^2\pi/8)$, has only 8 uniformly spaced non-zero coefficients with constant amplitudes and the phases $\{\pi/4, \pi/8, -\pi/4, -7\pi/8, \pi/4, -7\pi/8, -\pi/4, \pi/8\}$. Thus for M=64, if the original signal components are in the first 8 coefficients, the sequence of phase difference between the consecutive spectral replicas is $\{-\pi/8, -3\pi/8, -5\pi/8, -7\pi/8, 7\pi/8, 5\pi/8, 3\pi/8, \pi/8\}$. If the original signal coefficients are in the 9^{th} to 16^{th} coefficients, the phase difference sequence would be $\{\pi/8, -\pi/8, -3\pi/8, -5\pi/8, -7\pi/8, 7\pi/8, 5\pi/8, 3\pi/8\}$. Note that the position of the $-\pi/8$ phase difference is the location of the original signal component, and each entry in the sequence is unique. Thus, if we have two adjacent replicas of the modulated spectrum, we can reconstruct the filtered replicas of the spectrum by adding the replicas with appropriate phase shifts. The procedure for reconstructing the spectral replicas is explained next.

2.2 The details of step 14 (substitution method for SZ(8/64))

The spectrum S_1 consists of $M/4$ non-zero coefficients after applying the ¾ notch filter in step #10. Let the indices of these spectral coefficients be k to $(k+M/4-1)$. Note that the indices are cyclic and hence if any index exceeds M, subtract M from it to get the correct index. Of these $M/4$ coefficients, take any two separated by 8, i.e., i^{th} and $(i+M/8)^{th}$, and determine the phase of $S_1(i+M/8)/S_1(i)$. Now, compare this value with the eight values in the sequence, $\{\pi/8, -\pi/8, -3\pi/8, -5\pi/8, -7\pi/8, 7\pi/8, 5\pi/8, 3\pi/8\}$. The position of the closest match in the sequence is taken as the starting phase difference, and the rest of the entries are rotated cyclically to get the rearranged sequence. For example, if the calculated phase difference is closest to $-3\pi/8$, the rearranged sequence would be $\{-3\pi/8, -5\pi/8, -7\pi/8, 7\pi/8, 5\pi/8, 3\pi/8, \pi/8, -\pi/8\}$. Now, the coefficients at spectral indices $(i+nM/8)$; n=0,1,...7, are constructed by adding the phases in the above sequence to $S(i)$, of which the first two are already available. The rest are computed and inserted in the appropriate spectral places in the spectrum. This procedure is repeated for $i= k$ to $k+M/8$ which will reconstruct all the filtered coefficients.

A similar procedure can be followed for SZ(16/64) code.

2.3 Results of simulation and comparison of standard errors

The performance of the SZ-1 decoding algorithm using the magnitude deconvolution and the substitution method, in terms of the standard errors in the mean velocity and spectrum width estimates is obtained from simulation studies. The SZ(8/64) coded time series are simulated with different input velocities, spectrum widths, and overlay power ratios. The spectral parameters are estimated using the SZ-1 algorithm incorporating the deconvolution as well as substitution method. A large number of simulations are carried out to generate the statistics of the error estimates. The standard errors of the mean velocity estimate, v_2, and the spectrum width, w_2, of the weaker signal are compared in Figs. 2.1 and 2.2. The radar parameters used in the simulation are given in the figures. The curves are for w_2=2, 4, 6 and 8 m s^{-1}, respectively, starting with 2 m s^{-1} at the lowest. The continuous curves are for the deconvolution method and the dashed ones are for the substitution method. The curves are smoothed using a 5 point running average filter for clarity. The Fig. 2.1 is for mean velocity error, and Fig. 2.2 is for the spectrum width estimate error. It can be observed from the figures that, whereas the general trend is the same, the deconvolution method gives marginally better estimates than the substitution method, both for the velocity and the spectrum width. This difference is attributed to the manner in which the two methods reconstruct the weaker spectrum when the spectral replicas overlap. If the spectra overlap both methods are not exact but they work reasonably well for a single overlap of the spectral replicas.

2.4 Exact spectral reconstruction if the spectral replicas overlap onece

The substitution (and the deconvolution) procedure is exact only if the spectra are "narrow". If the spectrum spread is more than $1/8^{th}$ of the Nyquist interval, there will be overlapping spectral replicas which produce unequal amplitudes for the coefficients separated by 8 coefficients, and the phase difference will be arbitrary depending on the amplitude and phase of the overlapping signal components. Therefore, in the substitution method we have to compare the measured phase difference with the values in the expected sequence and choose the closest one. This is based on the assumption that one of the coefficients is small compared to the other, so that the phase difference is predominantly due to the stronger of the two overlapped coefficients. This assumption is

reasonably satisfied for the coefficients around the peak of the spectrum, but can lead to wrong phases at the tail ends of the spectrum.

In this section, we examine if it is possible to separate the two overlapping spectra. Further we assume that the spectra are overlapped once only, i.e., the non zero spectral coefficients are spread over $M/4$ coefficients, instead of $M/8$ coefficients. Here, we only give a theoretical analysis of the possibility of exact reconstruction. The additional computation is justified only if it yields substantial improvements in the width estimate. There is no possibility of further improvements in the velocity estimate by improved substitution. The velocity is estimated before the deconvolution in the SZ-1 algorithm, and reconstruction of the complete spectrum is not required for the velocity estimation. It is also mentioned in the report by Sachidananda et al. (1998, page 11, 2nd paragraph) that the velocity estimates worsen if it is obtained from the deconvolved spectrum. In general, any attempt to alter the spectrum results in a higher variance of the velocity estimate.

In order to explain the separation of the overlapped spectra, first we introduce the notation. Let S_1 be the spectrum after the notch filter is applied. For M=64, SZ(8/64) code modulation, and $3M/4$ notch filter width, it consists of only 16 non-zero coefficients. Let two of these non-zero coefficients, separated by $M/8$, be $S_1(i)$ and $S_1(i+M/8)$, and let these two coefficients have two original complex spectral coefficients, a and b, overlapping. Thus, we can write these two as a sum

$$S_1(i) = a \exp(j\phi_1) + b \exp(j\phi_2) ,$$

and

$$S_1(i+M/8) = a \exp(j\phi_2) + b \exp(j\phi_3) . \qquad (2.1)$$

The exponential multipliers are the coefficients of the convolution matrix, therefore, the phases, ϕ_i , i = 1,2,...8, are known. This gives us two equations with two unknowns, a and b which can be solved to obtain

$$a = [S_1(i) \exp(-j\phi_2) - S_1(i+M/8) \exp(-j\phi_3)] / [\exp(j(\phi_1-\phi_2)) - \exp(j(\phi_2-\phi_3))], \qquad (2.2)$$

and

$$b = [S_1(i) \exp(-j\phi_1) - S_1(i+M/8) \exp(-j\phi_2)] / [\exp(-j(\phi_1-\phi_2)) - \exp(-j(\phi_2-\phi_3))] . \qquad (2.3)$$

The only unknown in this procedure is one of the ϕ_i , i = 1,2,...8, to use in place of ϕ_1, ϕ_2, and ϕ_3 . Actually there is only one unknown because we know that the three phases are consecutive phases in the code sequence, hence we have to determine only ϕ_1 and the other two will follow from the sequence.

Now, we have to resort to the same procedure as before to determine the position of the phase difference between the two coefficients in the phase difference sequence $\{\pi/8, -\pi/8, -3\pi/8, -5\pi/8, -7\pi/8, 7\pi/8, 5\pi/8, 3\pi/8\}$. Find the closest match and build the sequence from that point onwards. We can also carry out an amplitude test to determine if the coefficient in question has overlay or not. If the two coefficients, $S_1(i)$ and $S_1(i+M/8)$, have different magnitudes then we know that there is overlay; the phase difference also will deviate from the one corresponding to the convolution code. We can only hope that one of the two overlaid signals is stronger so that we can resolve the correct phase difference. Once the two coefficients, a and b, are solved for, the complete set of 8 coefficients can be reconstructed very easily. This procedure can be applied to all the M/8 pairs present in the spectrum S_1 to restore all the M coefficients.

2.4 Conclusions

In this brief discussion, the magnitude deconvolution and the substitution methods are compared with respect to their performance in terms of the standard errors in the velocity and width estimates. Although both the velocity and width estimate errors are compared, it must be noted that the deconvolution method is used only for width estimation. The velocity estimation does not require the deconvolution. However, in the substitution method the velocity and width are estimated after the substitution, and hence we have compared the velocity errors also. Both methods perform well even if the spectra are not "narrow", but the deconvolution method performs marginally better, both with respect to the velocity and the width estimates.

3. Mean velocity estimation in the staggered PRT technique

Here, we describe the staggered PRT scheme briefly before we embark on a discussion of the method of processing. In the staggered PRT technique (Zrnic and Mahapatra 1985), two different pulse spacings, T_1 and T_2, are used alternately. Then,

alternate pairs of return samples are used to compute autocorrelation estimates, R_1 at lag T_1 and R_2 at lag T_2. The velocity is estimated from the phase difference between the two using the formula,

$$\hat{v} = \lambda \, arg(R_1 R_2^*) / [4\pi(T_2 - T_1)] \, . \qquad (3.1)$$

Thus, the difference in PRT, (T_2-T_1), determines the unambiguous velocity, v_a, for the staggered PRT technique and is given by

$$v_a = \lambda / [4(T_2 - T_1)] \; ; \; T_1 < T_2 \, . \qquad (3.2)$$

Zrnic and Mahapatra (1985) suggest a testing procedure to estimate mean velocity and signal power for echoes received within the time delay (T_1+T_2). In theory, this seems to be possible because the overlaid signals in any two consecutive samples are from two different ranges, and therefore are uncorrelated. Thus, the expected value of the overlaid signal contribution to the autocorrelation is zero, and the effective unambiguous range becomes

$$r_a = c(T_1+T_2)/2. \qquad (3.3)$$

Eq. (3.1) and (3.3) suggest that the staggered PRT is equivalent to a uniform PRT = (T_1+T_2) for the unambiguous range, and a uniform PRT = (T_2-T_1) for the unambiguous velocity; each can be selected independently. However, the practical utility of this scheme is limited due to the quality of estimates. The overlaid signal increases the variance of the estimates because it acts as noise. Thus, the ratio of the overlaid signal powers is the equivalent signal-to-noise ratio (SNR), and for a reasonable accuracy of the estimates, the unwanted signal has to be at least 3 dB below the desired signal power.

Let $r_{a1} = cT_1/2$, and $r_{a2} = cT_2/2$, such that $r_a = r_{a1} + r_{a2}$. If r_{a1} is chosen sufficiently large so that no echoes are received from ranges greater than r_{a1}, then the problem of overlaid echoes could be eliminated. For weather radars, r_{a1} would have to be 460 km (for 0.5 deg. elevation scan), but this would degrade the variance of the estimates

considerably. Thus, the practical limit for r_{a1} is smaller than 460 km unless some means of separating the overlaid signals is employed. It is possible to extend the unambiguous range to r_{a2} with some additional processing to resolve the one-overlay (i.e., alternate samples only have overlaid echoes) in some of the range locations.

It is shown by Zrnic and Mahapatra (1985), that the standard error in the velocity estimate increases as the ratio $\kappa = T_1/T_2$ approaches unity, and a good choice is κ =2/3. Thus, in practice, the unambiguous range and unambiguous velocity are restricted indirectly via the estimate accuracy. However, compared to the uniform PRT, it is possible to achieve a much larger r_a and v_a, because the limiting equation is $v_a r_{a1}$ equals $[(\kappa+1)/(1-\kappa)]c\lambda/8$ for the staggered PRT scheme without the overlay.

An alternative to the estimator (3.1), which results in a much lower standard error in the velocity estimate, is to use the phase of $R(T_1)$ for velocity estimation (aliased) and $R(T_2)$ for dealiasing or unfolding. If the ground clutter and overlay are not present, a pulse pair estimation of autocorrelations, $R(T_1)$ and $R(T_2)$, can be used for the estimation of spectral moments. The velocity estimator using the difference in phases of $R(T_1)$ and $R(T_2)$, (Eq. 7 of Zrnic and Mahapatra 1985), has a larger standard error because it uses the difference of two estimates. Sirmans et al. (1976) suggest use of either one of the autocorrelations for velocity estimation.

In our procedure, to obtain the correct velocity, we first compute two velocities, v_1 and v_2, using the phases of $R(T_1)$ and $R(T_2)$, from

$$v_1 = -\lambda \arg\{R(T_1)\} / (4\pi T_1),$$

and

$$v_2 = -\lambda \arg\{R(T_2)\} / (4\pi T_2). \qquad (3.4)$$

Now, assuming occurrence of one time aliasing, the possible velocities from the first estimate are v_1, and $(v_1 + 2v_{a1})$, or $(v_1 - 2v_{a1})$, whichever falls in the interval $\pm v_a$, and from the second estimate we have v_2, $(v_2 + 2v_{a2})$, and $(v_2 - 2v_{a2})$, where v_{a1} and v_{a2} are the unambiguous velocities corresponding to the PRTs, T_1 and T_2. Note that it is sufficient to consider a one-time aliasing for κ=2/3, because $v_a = 2v_{a1} = 3v_{a2}$. In these two sets of possible velocities, only one velocity, the correct one is common to both sets; it can be easily selected after comparison. In general, the velocities are estimates with certain

amount of error, hence we select the two closest, and then pick the corresponding value from the first set. The values from the first set have lower variances than the ones from the second set, because of the shorter PRT. This dealiasing procedure performs the best for κ=2/3, because the difference between the estimated velocities, $|v_1 - v_2|$, is the largest whenever there is aliasing. For effective dealiasing this separation must be larger than the standard error in the estimates. Thus, from the point view of large separation between these values κ=2/3 is also the best choice.

It can be inferred that for large signal spectrum width this unfolding technique is likely to fail (as do all other techniques), because the standard error increases with spectrum width. Therefore, the maximum width for which the unfolding is effective will be a certain fraction of the unambiguous velocity, but it is also a function of the number of staggered PRT samples, because the standard error decreases with increasing number of samples. We define a parameter called *loss* as the ratio of the number of times the unfolding failed to the total number of simulations. Sirmans et al. (1976) call this *loss* a "detection error rate" and compute it for staggered ratios ¾ and 4/5. In our simulation, the input velocity is varied uniformly over the entire $\pm v_a$ interval. The *loss* parameter is shown as a function of the normalized spectrum width in Fig. 3.1, where we have used 40 staggered PRT samples (approximately the same dwell time as in vcp-11 of WSR-88D) to generate simulated time series data for the figure. The PRT in the simulation is T_u = 0.61 ms with a v_a = 45.08 m s^{-1}. For M=40, the limit is about $w_{max} = 0.2v_a$, at which the *loss* is about 10%; i.e., the velocity is not correctly dealiased in 10% of the total number of simulations (about 2000 simulations). The *loss* is nearly zero up to about $w = 0.14v_a$ and then starts increasing rapidly. In the simulation study, the input velocities are spread over 90% Nyquist interval uniformly, leaving out the extreme ends. There is always velocity aliasing at the extreme ends that increases the *loss* by about 2% if 100% of the Nyquist interval is included. It is not included because this 2% does not reflect the performance of the dealiasing procedure. Our simulation results are consistent with the theoretical computations by Sirmans et al. (1976); their values of normalized spectrum width at which catastrophic errors occur are about twice as large as ours mainly because the number of samples in their computations is 2.5 times larger than herein.

A third alternative is to use the reconstructed uniform time series and use magnitude deconvolution procedure delineated in Report 3 (Sachidananda et al. 1999). In this procedure, the time series is made uniform with a period $T_u = T_1/2$ (for κ=2/3), by inserting zeros in place of the missing samples. This time series can be looked at as a product of the full time series and a code sequence of zeros and ones; zeros in place of missing samples and 1s in place of actual staggered PRT samples. The spectrum of this uniform time series is a convolution of the signal spectrum with the spectrum of the code, which has only five non-zero coefficients. Thus, the convolution produces a spectrum with five replicas of the original spectrum separated by $N/5$ coefficients, where N is the number of uniform samples. A magnitude deconvolution procedure can be used to restore the spectrum to the original shape, provided it is "narrow" ("narrow" spectrum is defined in Report 3). One can use this reconstructed magnitude spectrum to compute $R(T_u)$ from which we can get the velocity. This does not require unfolding provided T_u is chosen small enough.

From simulation we evaluated the standard errors in the velocity estimate using four methods. These are: (a) velocity from $R(T_u)$, i.e., uniform samples at intervals T_u, (b) velocity from $R(T_1)$ dealiased with the help of $R(T_2)$, (c) velocity from magnitude deconvolution, and (d) velocity from $\arg\{R(T_1)/R(T_2)\}$. We call the method (b) the staggered PRT pulse pair (ST) method. The various methods are compared in Fig. 3.2. Curve (a), the ideal case where all the samples at intervals T_u are available, is given for reference. The dwell time for all estimates is the same. The values are obtained using simulated time series and estimation of velocities by three different algorithms on the same (staggered PRT) time series. The simulation parameters are indicated in the figure. It is clearly seen that, of the staggered schemes, the method (b) gives the best estimate (curve # b in the figure), followed by (c) and (d).

The staggered PRT one-overlay resolution algorithm (henceforth labeled STO) presented in Report 4 uses the method-(c) if there is no clutter or the overlay. Because the staggered PRT pulse pair algorithm (method-(b)) performs better than the method-(c) in the absence of the ground clutter and the overlay, it is appropriate to replace the method-(c) by method-(b) in the overall schematic of the algorithm given in pages 34-36, Report 4. It is also important to change the thresholds on p_1/p_2 used for channeling the

computation, because the method-(b) performs differently than the method-(c). We have evaluated the ability of the staggered PRT pulse pair algorithm ST to estimate velocity in the presence of one-overlay. The largest p1/p2 ratio for which the pulse pair algorithm is effective in the presence of overlay is determined from simulations; this value is used in the algorithm to switch processing between the pulse pair algorithm ST and the overlay resolution algorithm STO. Because the algorithm is suggested only for the three elevations (2.4°, 3.35°, and 4.3°) of the WSR-88D vcp-11 (see Section 7), we have evaluated the *% loss* and $sd(v)$ as a function of the overlay power ratio, p_2/p_1, using the PRTs proposed for these three elevations. Simulations were carried out for four different spectrum widths of the signal, keeping the overlay signal spectrum width constant (w_2=4 m s^{-1}). The *loss* is nearly independent of the overlay signal spectrum width, w_2, hence, it is kept constant. The parameter *loss* is the number of times the velocity unfolding failed in 2020 simulations, with velocities spread over the entire Nyquist interval, expressed as a percentage. The $sd(v)$ is computed excluding the outliers (i.e., only the correctly unfolded velocity values are included).

Figs. 3.3 to 3.5 show the results of simulations for the three elevations, 2.4°, 3.35°, and 4.3°, respectively. It is apparent that as we decrease T_u (or increase v_a), the *loss* decreases up to a point and then reaches a limit. Note that all *loss* traces are more or less the same in Fig. 3.5 for all widths, but are spaced in Fig. 3.3. If we can tolerate a 10% *loss* for the weaker signal velocity, we can use a 6 dB cut-off for the overlay power ratio, i.e., apply the staggered PRT pulse pair algorithm ST to retrieve velocities of both signals if $|p_2/p_1| < 6$ dB. If it is larger than 6 dB, then we need the overlay resolution algorithm STO to recover the weaker signal velocity. The stronger signal velocity is always recoverable by applying the pulse pair algorithm (ST). Depending on the PRTs (dictated by the elevation angle) and the tolerable *loss,* the 6 dB limit can be lowered to 3 dB. An alternate choice could be 0 dB, in which case the stronger signal would always be processed by the ST pulse pair algorithm and the weaker one by the overlay resolution algorithm STO.

4. Clutter filtering and bias correction in the staggered PRT technique

A spectral domain clutter filtering and bias correction scheme is suggested by Sachidananda et al. (1999, Report 3). There the spectral coefficients of the weather signal, partially lost in the process of clutter filtering, are restored in amplitude using a magnitude deconvolution and multiplication by a coefficient determined from an approximate *initial* estimate of the velocity. During the course of reviewing this procedure, we found that it is possible to restore the complex coefficient exactly provided the spectrum is "narrow" as defined in the above referenced report. But, if the "narrow" spectra assumption is not valid then these two methods, viz., the magnitude only restoration and the exact complex restoration, behave somewhat differently with respect to the velocity estimate errors. It also requires more computation to restore the complex coefficients. Here we only give the mathematics of complex restoration procedure, and state the conclusions arrived at from simulation study. No simulation results are presented.

4.1. Restoration of the complex spectral coefficient and bias correction

The clutter filtering procedure is explained in the paper Sachidananda and Zrnic (2000), without the bias correction procedure, and the magnitude only restoration is explained in the Report 3 (Sachidananda et al. 1999). Here we shall use the same notation as in Report 3. To explain the complex coefficient restoration, let us start with Eq.(3.7), of Sachidananda et al. (1999)

$$\mathbf{V_r} = \mathbf{C_r}\,\mathbf{E_r}\,, \tag{4.1}$$

where $\mathbf{E_r}$ is the rearranged matrix of signal plus the clutter spectrum. Similarly, $\mathbf{C_r}$ is the rearranged convolution matrix, and $\mathbf{V_r}$ is the rearranged signal spectrum matrix after convolution. Assume that the ground clutter is around zero Doppler and the signal spectrum is "narrow". With this assumption, the first few coefficients in the first row and last few coefficients in the last row of $\mathbf{E_r}$ contain ground clutter. The non-zero signal coefficients are spread over only $N/5$ contiguous coefficients row wise; the position being determined by the mean velocity of the signal. Thus in any column of $\mathbf{E_r}$ a maximum of

two coefficients can be non-zero. Now, the convolution operation indicated by Eq. (4.1) spreads the clutter and the signal power present in each column of $\mathbf{E_r}$ into all the coefficients of the same column of $\mathbf{V_r}$. There is no shifting of the power from one column to another. Therefore, it is sufficient to consider one column of $\mathbf{V_r}$ and $\mathbf{E_r}$ to understand the signal restoration procedure. Let, the first column of $\mathbf{E_r}$ be $\mathbf{E_1} = [a, 0, 0, b, 0]^t$, where a is the clutter coefficient, and b is the signal coefficient; both complex. After the convolution, the first column of $\mathbf{V_r}$, **A,** is given by

$$\mathbf{A} = \mathbf{C_r}\,\mathbf{E_1} = a\,\mathbf{C_1} + b\,\mathbf{C_4}\,, \tag{4.2}$$

where $\mathbf{C_1}$ and $\mathbf{C_4}$ are the 1st and 4th columns of the convolution matrix, $\mathbf{C_r}$. After the clutter filtering (Eq. 3.11 of Sachidananda et al. 1999) the first column of $\mathbf{V_f}$ can be written as

$$\mathbf{B} = \mathbf{A} - \mathbf{C_1}^{t*}\mathbf{A}\mathbf{C_1}\,. \tag{4.3}$$

Substituting for **A** in (4.3) and simplifying, we can reduce it to

$$\mathbf{B} = b(\mathbf{C_4} - \mathbf{C_1}^{t*}\mathbf{C_4}\mathbf{C_1}). \tag{4.4}$$

Note that the clutter coefficient, a, is completely deleted by the clutter filtering, but the signal coefficient, b, is multiplied by a complex known vector. Now, to get back the signal vector, $b\mathbf{C_4}$ present in **A**, we carry out the matrix operation given by

$$b\mathbf{C_4} = (\mathbf{C_4}^{t*}\,\mathbf{B}\,\mathbf{C_4}) / (1 - |\,\mathbf{C_1}^{t*}\mathbf{C_4}\,|). \tag{4.5}$$

This procedure is carried out on the first few columns of $\mathbf{V_f}$ from which clutter is filtered to restore the signal vector.

In this illustration we have assumed that the signal coefficient is in the 4th position in $\mathbf{E_1}$. In general the position of the signal coefficient can be any one of the five, hence a general expression can be written as

$$b\mathbf{C}_k = (\mathbf{C}_k^{t*}\,\mathbf{B}\,\mathbf{C}_k) / (1 - |\,\mathbf{C}_1^{t*}\mathbf{C}_k\,|^2), \qquad (4.6)$$

where k is the position of the signal coefficient which is determined from the *initial* velocity estimate. The index k can be different for different columns of $\mathbf{V_f}$ depending on the *initial* velocity. The *initial* velocity is estimated using the magnitude deconvolution procedure on the filtered spectrum, $\mathbf{V_f}$, before restoring the signal components lost during the clutter filtering. For the last few columns of $\mathbf{V_f}$, the clutter coefficient is in the last row, hence $\mathbf{C_1}$ is replaced by $\mathbf{C_5}$ in (4.6) while restoring the signal in these columns. Note that in (4.6) the denominator is zero if k =1, which corresponds to the signal having near zero Doppler. The signal is completely filtered out, and the numerator also would be zero in this case. In the actual radar time series processing, however, the numerator would not be zero because the signal spread is not "narrow" in the strict sense. Thus, we cannot restore the signal if the Doppler is near zero as in the previous method.

If the assumption of "narrow" spectra is strictly valid, then both methods of signal restoration, viz., the magnitude only restoration and the complex restoration, are exact, and give the same spectral moment estimates. However, if the spectra are not "narrow" the two methods differ in performance to some extent. The magnitude restoration performs slightly better than the complex domain restoration in the presence of overlapping spectral replicas, and also requires less computation. We have examined the performance of these two methods using simulated time series, however, no results are presented because the complex restoration did not fare better than the magnitude only restoration explained in Report 3. The results for the magnitude only restoration are available in that report.

5. Ground clutter filtering and the window: some considerations

The ground clutter is usually present in the lower elevation scans approximately in the in the first 20 km from the radar. At elevations higher than about 5° the ground clutter is not a serious problem. The WSR-88D specifies a 50 dB rejection for the ground clutter (at 0.5° and 1. 5° elevation) with a spectrum width of 0.28 m s^{-1} centered on zero Doppler. We use this width for the ground clutter in our simulation study, and use clutter-

to-signal ratio (*CSR*) as a parameter rather than the clutter rejection. We adopt this notation because our ultimate aim is to recover the spectral moments of the weather echo, and to achieve this, it is sufficient to filter enough clutter power to obtain a sufficient *SCRR* (i.e., Signal to Clutter Residue Ratio) so that the spectral moment estimates are accurate. The amount of filtering required depends on the *CSR*. Further, the clutter suppression (or rejection) ratio, α, defined as the ratio of the total clutter power to the residual clutter power after filtering, expressed in dB units, is a function of the filter width, hence any suppression can be obtained by suitably choosing the filter width. But this does not guarantee recovery of spectral moments of the weather signal, because there is an upper limit for the filter width beyond which the velocity cannot be recovered irrespective of the *CSR*. This is because the *initial* velocity estimate (required for bias correction or the signal restoration) is obtained from the residual signal coefficients only after clutter filtering. There is always an optimum clutter filter width for a given *CSR* and a clutter spectrum width. If the clutter filter width is allowed to be adjusted in the staggered PRT decoding algorithm based on an a-priori knowledge of the *CSR* (we can use a clutter map), the performance of the algorithm can be optimized. It is obvious that the residual clutter power is spread throughout the spectrum and hence can be treated as noise. Thus, the *SCRR* after filtering the ground clutter is equal to (α - *CSR*) dB, neglecting the noise power (or assuming the noise power to be very small compared to the residual clutter power). This has to be better than 10 dB to recover velocity of the weather echo with a good accuracy. Other parameters that play important roles in the clutter filtering are the window function and the number of available staggered PRT samples, *M*, because the suppression ratio is a strong function of the these two parameters. All these aspects were discussed in Section 3.3.2, of Sachidananda et al. (2000, Report 4). Here we consider an aspect of the clutter filtering which was not included in that discussion, i.e., the recovery of the spectral moments (specifically the mean velocity) when the signal spectrum is very narrow and is overlapping the clutter spectrum. The overlapping happens if the mean velocity is near or at 0, $\pm 2v_a/5$, or $\pm 4v_a/5$, for κ=2/3.

In this specific case, the *SCRR* after the ground clutter filtering is not equal to (α - *CSR*) dB for the *initial* velocity estimation, because the signal is also filtered along with

the clutter. The above formula is valid only if the signal and clutter spectra do not overlap. If the signal and clutter spectra overlap, the ability to achieve a *SCRR*>0 dB after filtering depends on the relative spectrum widths of the clutter and the signal, and the manner in which the signal and clutter power fall as a function of the clutter filter width. For velocity recovery, the first condition is that the signal spectrum width must be larger than the clutter spectrum width, so that the rate at which the residual signal decreases as a function of the clutter filter width is slower than the rate at which the residual clutter decreases. Only under this condition the *SCRR* increases as a function of the clutter filter width, and can become greater than zero for sufficiently large width.

The window function is very critical in achieving *SCRR*>0, because it changes side lobe structure of the spectrum. While a rectangular window has very large side lobes, there are windows that produce very low side lobes. We have examined the effect of different windows and found that we can capture most of the effects by considering a window of the type $\{\text{von Hann}\}^n$, where the exponent '*n*' controls the side lobe level; larger the *n*, lower is the side lobe level, of course, with a wider main lobe. The power loss due to the window also is higher with increasing *n*, which affects the variance of the estimates. Fig. 5.1 shows the residual *CSR* after the clutter filtering using different *n* values for the $\{\text{von Hann}\}^n$ window. Note that *SNR* after clutter filtering is the inverse of the residual *CSR* (or negative of the *CSR* in dB.) The overlapping signal spectrum width is assumed to be 1 m s^{-1}, and the clutter spectrum width is equal to 0.28 m s^{-1}, *CSR* = 50 dB. The weather signal and clutter spectra are simulated, and different clutter filter widths are used in computing the residual *CSR*. The spectral domain notch filter width n_c can be changed in steps of one coefficient at a time (hence the width depends on the number of samples or dwell time). The number of samples is *N*=160 (*M=64*), and it should be noted that the achievable *SCRR* also depends on the number of samples. Further, it can be observed that the residual *CSR* initially decreases to a lowest value and then starts increasing. From the figure it follows that a minimum $n = 2$ is required to achieve a residual *CSR*<0 dB. The figure also suggests that $n = 4$ achieves a better *CSR* than is possible with *n*=2, but with a slightly wider clutter filter width. The results of a simulation study using staggered PRT processing on a simulated time series with $w = 1$ m s^{-1} and a *CSR* = 50 dB (w_c=0.28 m s^{-1}) are shown in Fig. 5.2 ($\{\text{von Hann}\}^2$ window and

n_c = 9) and in Fig. 5.3 ({von Hann}^{4} window, same time series). It can be seen that whenever the signal and clutter spectra overlap (i.e., for $v = 0, \pm 2v_a/5$, or $\pm 4v_a/5$), use of the {von Hann}^{2} can not recover velocity effectively but application of the {von Hann}^{4} window can. Thus, for large *CSR* and narrow signal spectrum it is advantageous to use {von Hann}^{4} window. For lower *CSR* or wider signal spectra {von Hann}^{2} is generally sufficient, and better in terms of the $sd(v)$.

The inherent rectangular window spreads clutter power across the spectrum giving a low value of clutter suppression ratio, α. There is a signal power loss associated with the window, which increases the standard error in the mean velocity estimate. Note that for the signal velocity estimation, it is sufficient to make (α–*CSR*) < –10 dB approximately. For a given N and clutter filter width, the exponent n must be selected such that we can achieve an $\alpha >$ (*CSR*+10) dB. A higher n will allow a lower filter width, but with associated signal loss. The signal power loss can be computed from the weighting function directly as 4.23 dB, 5.67 dB, and 7.03 dB, for n = 1, 2, and 4, respectively.

The clutter suppression ratio, α, is very sensitive to the number of samples M (or N). Thus, increasing the number of samples achieves a higher α for a given window. We observe that higher the order of the window (i.e., larger n), more samples at both ends of the sequence are suppressed, and do not significantly contribute to the estimate. Although the number of samples available from a radar is limited by the allowable dwell time, we can increase N by simply adding zeros at both ends of the sequence, which are going to be suppressed anyway by the window function. Higher the order of the window, more zeros can be added. If we use a criterion that the side lobe level of the spectra should not be altered significantly by adding zeros, the number of zeros that can be added are about 14, 33, and 76 percent of the available samples for the window exponent, n = 1, 2, and 4, respectively. (The {von Hann}^{n} window is applied to the augmented time series, i.e., the series that has been padded with zeroes.) These percentages are calculated from the window weights and verified using simulation. This also reduces the signal loss due to the weighting to about 3.5 dB in all three cases, from that indicated in the previous paragraph, and hence allows us to achieve a higher α without sacrifice of the estimate error. This is a significant result, and is worth testing on a radar. Simulation results (not

presented here) show that a {von Hann}^{4} window applied to a 76 percent lengthened sequence by adding zeros, allows to recover velocity accurately for a *CSR* as high as 50 dB with 50 staggered PRT samples, for the case signal spectrum with w=1 m s^{-1} overlaps the clutter.

6. Testing of the staggered PRT algorithm on actual radar data

The WSR-88D research radar at NSSL has a capability to record the time series data either through the new RDA (at all range gates) or the SIGMET processor (at about 100 contiguous range gates). Although, the staggered PRT mode is not programmed in yet, we have collected some uniform time series data (through the SIGMET processor) with the shortest PRT available in vcp-11 of the radar (PRT # 8; T_u = 0.78 ms; r_{au} =117 km; v_{au} = 35.25 m s^{-1}; the subscript '*u*' is used to denote uniform PRT). Some data are recorded with the antenna stationary so that the statistics of the actual spectral parameter estimates could be obtained, and others with a scanning antenna. Some are with clutter and weather, and there are some with overlay.

The staggered PRT sequence with κ =2/3 is derived from this sequence by dropping samples (drop 2nd, 4th, and 5th samples in every 5). Thus, for the "derived" staggered PRT sequence T_u is 0.78 ms (T_1=1.56 ms, T_2 = 2.34 ms), which gives twice the unambiguous range, r_{a1} = 234 km, and the same unambiguous velocity, v_a = 35.25 m s^{-1}. This, of course, is not exactly same as transmitting a staggered PRT sequence, because if there is weather at ranges greater than r_{au}=117 km the samples can have overlay. The overlay is eliminated in the true staggered transmission if the weather is confined up to twice r_{au}. There is an advantage in testing the staggered PRT scheme in this manner, which is, in the absence of overlay the uniform PRT sequence serves as a reference sequence, as we have in the case of simulated time series. The spectral parameters and their variances, estimated using the uniform sequence, can be compared with the corresponding parameters from the staggered PRT sequence, which uses only 2 out of 5 samples of the uniform sequence. We can get a qualitative feel for the extent of degradation in the estimate accuracy using the staggered PRT scheme, while getting a larger unambiguous range; twice the range with pulse pair processing with no overlay, and three times the range with overlay resolution algorithm. The T_u = 0.78 ms is large for

the staggered PRT scheme, because the unambiguous velocity is not sufficiently large to satisfy the "narrow" spectra criteria required for clutter filtering algorithm, but it is expected to work reasonably well for signals with spectrum widths of about 4 m s^{-1} or less.

We have used three different algorithms to process the time series. (a) The pulse pair algorithm on the uniform time series (without and with clutter filter) implemented in the spectral domain, (b) the pulse pair algorithm, ST, on the "derived" staggered PRT time series without the clutter filtering, and (c) the spectral domain processing of the staggered PRT with the clutter filtering and bias correction. For the staggered PRT scheme the algorithm (b) is to be used if there is no clutter or overly, and the algorithm (c), if ground clutter is to be filtered. The algorithm (a) provides the reference to compare the estimates and their errors using the other two algorithms. The one-overlay resolution algorithm could not be tested using this method, because it needs the time series from a true staggered PRT transmission. Although, several sets of data are collected, only a selected few are presented in this report. The specific cases are selected to highlight the strengths as well as the weaknesses of the staggered PRT algorithms: the pulse pair and the spectral domain clutter filtering algorithms.

Case-1: date 05:28:2001, time 03:35:40

This set of time series data was collected on May 28, 2001 using the Sigmet digital receiver. The antenna was stationary at 246.66° azimuth and 0.26° elevation. The range covered is from 19.5 km to 32 km with a gate spacing of 0.25 km. The time series length per radial is 256 samples for all the 51 gates. The number of samples is large, but, in the actual operation (the vcp-11 scan) the dwell time per radial is about 50 ms.

To generate the statistics of the velocity estimates, we have chopped the time series into four pieces of 64 samples each (dwell time of about 50 ms per estimate). With the antenna stationary, about 40 estimates were obtained for each range bin in about 2 seconds, which is a reasonably small time so that the effects of advection and evolution of weather phenomena should be negligible. The uniform PRT of 0.78 ms is used, which gives an unambiguous velocity of 35.256 m s^{-1}. With this unambiguous velocity we can expect to estimate the mean velocity accurately using the staggered PRT pulse pair

algorithm (if clutter is not present) for widths up to about 5 m s^{-1}. The staggered PRT clutter filtering algorithm requires that the number of uniform PRT samples, N, be divisible by 5, hence, we have used 60 uniform samples, or 24 samples for the derived staggered PRT sequence.

In this data set clutter is present only at a couple of locations, but the rest of the regions have only weather. Figure 6.1 shows a scatter plot of the mean velocities of all the 51 range bins, estimated using the pulse pair algorithm on the uniform PRT sequence. Each estimate is represented by a dot, and there are 40 estimates at each of the 51 range bins. The mean and the standard deviation are also shown with continuous and dashed traces, respectively. It can be observed that there is some ground clutter at 23 and 26 km, where the velocities appear to be biased towards zero because of the clutter.

In figure 6.2 is a plot of all the three spectral parameter estimates along a radial for one dwell time from the same data set. The four traces in each of the three plots in the figure correspond to the estimates obtained using the four methods indicated by the abbreviations shown in the legend. The abbreviations stand for: (a) uPRT:PP – the uniform PRT sequence processed using the pulse pair algorithm without the clutter filter, (b) uPRT:CF – the uniform PRT sequence processed using the pulse pair algorithm after the clutter filtering (The clutter filtering is implemented in the spectral domain.), (c) stPRT:PP – the derived staggered PRT sequence processed using the staggered PRT pulse pair algorithm (uses $R(T_1)$ for aliased velocity, and $R(T_2)$ for dealiasing; no clutter filtering is used), and (d) stPRT:CF – the derived staggered PRT sequence processed using the staggered PRT clutter filtering and the bias removal algorithm. It can be seen that all four traces nearly merge for all the ranges except where the clutter is present. A comparison of velocity estimates around 26 km indicates that the staggered PRT clutter filtering is effective in extracting the velocity information (dashed trace). The CSR is small; about 6 dB at this location as can be inferred from the mean power estimate plot before and after clutter filtering. The overall matching of the traces indicates that the estimates from the derived staggered PRT sequence, which uses only 2 out of 5 samples of the uniform PRT sequence, compare well with the ones from the uniform time series. The estimates in this plot are obtained from the full time series of 256 samples. The staggered PRT pulse pair algorithm also works well if the clutter is absent and the

spectrum width is not excessive. It may be noted that the spectrum widths in this data set are less than 4 m s^{-1}, which is within the limit of $0.14v_a$.

Figure 6.3 shows the spectra of the signal along the same radial whose spectral parameters are shown in Fig. 6.2. We can clearly see the signal spectra with positive velocity varying between 10 to 20 m s^{-1}; the ground clutter is seen around 20.5 km, 23 km, and 26 km. The data set is processed using the pulse pair algorithm after the clutter is filtered. The clutter filtering is implemented in the spectral domain, with n_c =7 (n_c is the number spectral coefficients deleted around zero Doppler), and the number of samples is 64. The resulting velocity estimates are shown in the scatter plot (Fig. 6.4); the mean and the standard deviation are also shown. The clutter is clearly removed. This figure can be used as a reference to compare with the estimates obtained from the derived staggered PRT sequence.

The next plot (Fig. 6.5) is a scatter plot of velocities from the derived staggered PRT sequence processed using the pulse pair algorithm. Comparing this with Fig. 6.4, we can see that the estimates are as good as the uniform PRT estimates, except in places where there is clutter. The standard error also compares well as can be seen from the spread of the estimates. Clutter filtering is not possible in this method.

In Fig. 6.6 is a similar scatter plot obtained from the derived staggered PRT sequence but including the clutter filtering and bias correction algorithm. The first observation is that the variance of the estimates is a little larger than the variance of estimates obtained with the pulse pair algorithm. The $sd(v)$ is about 1.5 m s^{-1} for ranges less than 22 km, and about 1.0 m s^{-1} for ranges greater than 27 km. Between 23 and 26 km the error is large because dealiasing is incorrect in some of the estimates. The increase in the standard error is due the overlap of the spectral replicas.

Case-2: date 05:28:2001, time 02:55:10

The next case that we have selected is with a strong ground clutter. The time series data was collected on May 28, 2001 with the antenna stationary at azimuth 319.83° and elevation 0.23°. The data was recorded for about 2 seconds with a uniform PRT of 0.78 ms, and 256 samples per radial. As in the previous case we took all the 256 samples to compute and plot the spectra, but for generating the statistics of the estimates, we have

used a dwell time of 50 ms (64 samples) for each estimate. In Fig. 6.7 all the three spectral parameter estimates are shown for one radial. From the mean power plots with and without the clutter filter, we can see that there is large ground clutter throughout; from 6 to 18 km. The CSR is as high as 30 dB in some places. The corresponding velocity traces show that without the clutter filter the velocities are heavily biased towards zero. However, after clutter filtering, the velocity estimates from the uniform PRT sequence as well as derived staggered PRT sequence agree very well in most of the range bins, except between 14 and 16 km. The reason is obvious from the spectrum width plot (Fig. 6.7); the width is more than 10 m s^{-1} in this region (see width trace for uPRT:CF). The "narrow" spectra criterion is not satisfied for the echoes from these ranges. The spectra along the same radial are plotted in Fig. 6.8. This is a clear case of overlaid signal from the second trip. Although the overlay is present throughout, the overlay power relative to the signal power is large only for ranges beyond about 11 km. The combination of the signal plus the overlay has very large spectrum width, hence, the clutter filtering algorithm fails for these range bins. Note that the performance for a true staggered sequence would be better because the overlaid signal occurs within one PRT, hence it is incoherent with respect to the first trip signal. The next two scatter plots (Figs. 6.9 and 6.10) clearly show that the staggered PRT clutter filtering and bias correction algorithm has performed very well up to 12 km (compare the two figures, Fig. 6.9 is the reference using the uniform PRT sequence).

Case-3: date 05:29:2001, time 14:17:50

This data set was collected with the antenna stationary at 240.6° and elevation 0.17°. The ranges covered are 26.25 km to 38.75 km. We have selected this data set to show the failure of the staggered PRT pulse pair algorithm caused by the presence of wide spectra. The ground clutter is mostly absent, except for ranges less than 28 km. In Fig. 6.11 is a plot of the spectral parameter estimates for one radial. The first plot shows that all four mean power estimates are nearly the same for ranges greater than 28 km, which indicates that there is no clutter; i.e., the power estimate before and after clutter filtering is the same. Between 27 and 28 km there is clutter with a CSR of about 40 dB. From the velocity estimate trace (second plot) it can be seen that the staggered PRT

clutter filtering algorithm performs much better than the pulse pair algorithm (compare dashed trace with dotted trace), although the ground clutter is not present. The reason is the spectrum width, which is nearly 10 m s^{-1}, as seen from the width plot. The spectra plot along the radial (Fig. 6.12) shows the spread of the power. This also appears to be a case of 1st and 2nd trip overlay. The next three figures are the scatter plots of velocity estimates using the uniform and the derived staggered PRT sequences. Comparing the Figures 6.14 and 6.15 with Fig. 6.13, it is clear that both staggered PRT methods have failed miserably in this case because of the large spectrum width. From Fig. 6.11 and the extended unambiguous velocity of 70.1 m s^{-1} one can see that the normalized spectrum widths are larger than 0.1. Thus, according to Fig. 3.1 the percentage of lost estimates can exceed 20%. Further, the standard error of estimates increases abruptly (curve b in Fig. 3.2) if the normalized spectrum width is larger than 0.07 (i.e., 8/110). Both these effects contribute to the failure.

Case-4: date 05:28:2001, time 03:31:10

This data set was collected with a scanning antenna. The scan rate was 19° per second, which is about the same as in vcp-11 of the WSR-88D. The number of samples per radial is 64 (dwell time about 50 ms) and the time series data is processed using the four methods discussed in this section; i.e.,(1) uPRT:PP, (2) uPRT:CF, (3) stPRT:PP, and (4) stPRT:CF. PPI displays are generated for the mean power, the mean velocity and the spectrum width (Figs. 6.16 to 6.18). In each figure there are four PPI sectors of fields from the same location separated by a small gap (black, white or gray). They correspond to the estimates obtained using the four methods. The color bar on the right indicates the categories used in the display. Because of coarse color coding these figures only give a qualitative feel for the performance of the four algorithms; finer variations are masked by the effects of quantization. The ground clutter is present only in a few locations (see display #1 in Fig. 6.16) indicated by the red spots, which are eliminated after the clutter filtering (display #2 in Fig. 6.16).

The powers in #1 and #3 agree quite well (Fig. 6.16) as expected. In #3 there are less samples per estimate, but the dwell times are the same hence a very small difference

in the sd(p) makes the fields almost indiscernible. Equally good comparison is between the fields #2 and #4, which are obtained from clutter filtered data.

The velocity displays #1, #2, #3, and #4 are nearly the same in Fig. 6.17, except for some regions where the staggered PRT pulse pair and the clutter filtering algorithms have failed. At these places the spectrum width is large (see Fig. 6.18, display #2).

It appears that clutter filtering generally decreased the spectrum widths while preserving the main features of the fields (compare #1 and #3 or #2 and 4 in Fig. 6.18).

7. Revised vcp-11 scan strategy for the WSR-88D

Since the submission of the Report 4, we have examined several outstanding issues that were left out in the course of the range-velocity ambiguity resolution studies carried out at NSSL. Some of these are addressed in this report. In view of these new inputs we have revised the table 5.2 of Report 4 and added some more information.

During the course of our discussions on the selection of PRTs, it was determined that the shortest PRT is restricted to 0.705 ms by the pulse forming network (PFN) charging circuit in the transmitter of WSR-88D. Hence, the shortest T_u that can be used in the staggered PRT mode with a κ=2/3 is 0.3525 ms. We have modified the PRTs for the higher elevations because of this limitation. The wavelength of the research and development WSR-88D radar in Norman is 11 cm, which causes a 10% increase in the unambiguous velocity compared to the λ=10 cm used in the earlier table. The exact value for each WSR-88D will depend on the specific frequency allocation and thus will be between the values in these two tables.

The second important observation is that, in the absence of overlay and the ground clutter, the spectral parameters can be estimated using the pulse pair algorithm. In this scheme the autocorrelations $R(T_1)$ and $R(T_2)$ are used to compute two aliased velocity estimates, which can be easily dealiased in the $\pm v_a$ interval corresponding to T_u. It is shown in Section 3that the spectral moments estimated using this method have much lower errors than using the formulae in Zrnic and Mahapatra (1985). It is important to note that most of the area scanned by the radar falls in this category, and only a small fraction of the area, especially in the low elevation scans, is contaminated by the ground clutter and/or overlay. Thus, the clutter filtering algorithm and the overlay resolution

algorithm, discussed in Report 3 and 4, respectively, can be selectively applied in these regions. Because the overlay resolution algorithm STO uses spectral domain processing (FFT) and thus, requires significantly more computation than the pulse pair algorithm, we have tried to minimize the use of overlay algorithm to the extent possible. The PRTs are selected such that the overlay algorithm might be required only for selected regions at the three lower elevation scans (2.4°, 3.35°, and 4.3°), where the overlay can occur. Even in these three scans the decision to apply the overlay resolution algorithm can be made using the long PRT scan reflectivity data available from the 1.45° elevation scan. The ground clutter is typically confined to the lower elevations (below 5°), and the decision to apply the clutter filtering algorithm can be made based on the clutter map and identification of anomalous propagation. Both the overlay resolution and the clutter filtering algorithm require FFT processing, however, for the major part of the area scanned by the radar, pulse pair processing is sufficient.

The staggered PRT scheme increases the unambiguous velocity compared to the uniform PRT. In the absence of the ground clutter and the overlay, the computation required for the pulse pair processing (ST(2/3)) is less than that for a uniform PRT transmission (computation of two autocorrelations are needed, but with 1/5th the number of multiplications each). Thus, for elevations higher than about 5° for which the ground clutter is almost absent, the staggered PRT is recommended all the way up to 19.5°. Because of the restriction on the shortest PRT (0.705 ms) that the transmitter can handle, for elevations 10° and above we have selected the T_u =0.36 ms, although shorter PRTs would further increase the unambiguous velocities.

Tables 7.1a and 7.1b show the selected PRTs and other parameters for the vcp-11 of the WSR-88D. The azimuth rate and scan period is from the original WSR-88D vcp-11 (see Table.5.1a, Report 3). The beam width of the antenna is 0.9°, thus there are 400 radials in 360° from which the dwell time is computed using the scan period. The type of transmission is indicated in column-5. The CS,1 corresponds to the contiguous surveillance scan using PRF#1 (PRT=3.11ms). This is the long PRT scan from the original vcp-11 of the WSR-88D without any change. This is followed by a SZ(8/64) coded scan which replaces the CD (contiguous Doppler) scan. The abbreviation STO(2/3) stands for staggered PRT with one-overlay resolution, and ST(2/3) is the staggered PRT

without the overlay resolution. The STO(2/3) scan is recommended for only three elevations (2.4°, 3.35°, and 4.3°). The PRTs selected for each of the scans are listed in columns 6 to 8. It can be seen that the lowest PRT (0.72 ms) is within the transmitter capability. The number of available staggered PRT samples, M, is computed from the dwell time and the PRTs. The maximum range, r_{max} to which the proposed mitigation technique applies is calculated by assuming that the maximum storm top is about 18 km for all elevations, except for 0.5°, for which 16 km height is used. We are able to achieve the required range (r_{a2} with overlay resolution, r_{a1} without overlay resolution) for all elevations except 2.4° for which it is about 30 km short.

The schemes for the first two elevation scans are the same as before; long PRT for reflectivity up to a range 460 km, followed by a short PRT with SZ(8/64) phase coded transmission. The SZ(8/64) phase coding gives a range of 234 km with an overlay resolution capability of $|p_1/p_2|$ up to 20 dB for $w_1 = w_2 = 4$ m s^{-1}; i.e. it can resolve spectral parameters of the first two trip signals overlaid. With some modifications to the SZ-1 algorithm, it is possible to resolve overlay of any two of the four possible trip overlays up to the range of 460 km.

The staggered PRT mode is recommended for all the elevations 2.4° and higher with the PRTs listed in columns 7 and 8. The overlay resolution algorithm has to be applied to elevations 2.4°, 3.35°, and 4.3°, whenever there is overlay within the longer PRT (between ranges 0 and $r_{a1}/2$, and ranges r_{a1} and r_{a2}); else the pulse pair algorithm should be applied. The clutter filtering algorithm is to be applied for ranges 0 to $r_{a1}/2$, wherever the ground clutter is indicated by the clutter map. The extended range with overlay resolution, r_{a2}, is indicated only for these three elevations. The last column lists the unambiguous velocity for the selected PRTs.

Note, if ground clutter from distant ranges (i.e., r_{a1} to r_{a2}) is the overlaid echo, the filtering algorithm should be somewhat modified. We have not addressed the modifications because they are needed for distant regions where ground clutter is normally absent. Anomalous propagation and mountains can produce clutter at large range hence this issue will be examined in subsequent studies.

Table 7.1b lists all the standard errors obtained from simulation studies for three different spectrum widths. The two values for the SZ(8/64) phase coding scheme is for

the 1st and the 2nd trip echoes, after separation. It is assumed that the 1st trip is stronger and the 2nd trip is weaker, with a ratio p_1/p_2 = 20 dB. If the situation is reversed the standard error values are to be interchanged. The values for the staggered PRT scheme are from pulse pair algorithm (ST), without the ground clutter or the overlay. The performance with clutter filtering and the one-overlay resolution is given in later tables, however, this table is an indicator of the overall performance of the proposed vcp-11 strategy, because most of the time the pulse pair algorithm, ST(2/3) is sufficient for the staggered PRT scans. The standard errors are nearly the same as for the original vcp-11 of WSR-88D (compare the values in Table. 5.1c of Report 3, for w=4 m s^{-1}), and are well within the acceptable limits. An added advantage is that the unambiguous velocities are much larger (compare the v_a values in Table 5.1c of Report 3 with those in Table 7.1a) without compromising the unambiguous range.

Next we discuss the reasoning that went into the selection of PRTs for each of the elevations. Because the one-overlay resolution algorithm, STO(2/3), uses FFT, we have tried to minimize the use of this algorithm, and restricted it to only three elevations, 2.4°, 3.35°, and 4.3°. We examined several possible PRTs for each elevation, keeping in mind the maximum range required for avoiding overlay. Table 7.2 lists the standard errors in the spectral moment estimates for several selected PRTs (i.e., T_u) and each of the elevation scans of the vcp-11 in which the pulse pair algorithm, ST(2/3), is applied. It is assumed that there is no overlay or ground clutter, hence r_{a1} is the slant range within which the scatterers are located. The shortest PRT is selected to achieve the required range, r_{max}, with one-overlay resolution; the longest PRT has no overlay in the three elevations, 2.4°, 3.35°, and 4.3°. For 5.25° and higher, we can select a PRT to satisfy the range requirement without overlay. The table also lists the *loss* parameter (below the $sd(v)$ in the same column), i.e., the number of times the unfolding of the velocity failed, expressed as a percentage of the total number of simulation trials. This parameter is given only if it is significant; values less than 1% are ignored, as they are due to the aliasing at the ends of the $\pm v_a$ interval. Note that the $sd(v)$ listed is computed from the correctly resolved velocity values. This approach is used because, whenever there is a wrong dealiasing, the velocity value is off by $2v_{a1}$, and the $sd(v)$ suddenly jumps to a large value, unrepresentative of the standard error.

The selection of PRT is a question of compromise between the ability to estimate velocity accurately and the computational complexity. For example if we select T_u=1 ms for the 2.4° elevation, we would get the required range of 303 km without using the one-overlay algorithm, but the ability to estimate velocity is restricted to signals of width less than about 3 m s^{-1}. Simulations indicate the *loss* = 7.5% for w = 4 m s^{-1}, and the *loss* = 37.9% for w = 6 m s^{-1}. The unambiguous velocity, v_a = 27.5 m s^{-1} is not large enough to satisfy the "narrow" spectra (normalized) criteria; thus the clutter filtering also will fail even for CSR as low as 20 dB (see later discussions of Tables 7.3 and 7.4). Thus, for effective clutter filtering as well as for one-overlay resolution, a PRT corresponding to T_u = 0.61 ms is the optimum choice for 2.4° elevation (Table 7.2), although we have to slightly relax the range requirement. Having selected this PRT, it is necessary to use overlay resolution algorithm if there is weather beyond 183 km. Similarly, for the next two elevations, with the selection of the PRTs corresponding to T_u = 0.82 ms, and 0.69 ms, respectively, we can bypass the overlay resolution algorithm, but at the expense of the velocity recovery. The *loss* is 18% and 4.6% for w = 6 m s^{-1}, respectively, at the two elevations. Therefore, we have selected shorter PRTs (i.e., T_u = 0.55 ms for 3.35° and 0.46 ms for 4.3°, Table 7.1b) for which the one-overlay resolution algorithm would be used to achieve the required range in regions where the overlay is present.

The ground clutter filtering is important for the close ranges and low elevations. The next few tables summarize the performance of the clutter filtering algorithm for each of the elevations, taking into consideration the PRTs, number of samples, etc. We have set the clutter spectrum width w_c to 0.28 m s^{-1} in all our simulations, and all the results presented in Tables 7.3 and 7.4 are for this value. The signal spectrum width is 4 m s^{-1}. There is an optimum clutter filter width and a window function for each clutter-to-signal ratio (CSR) which provides the best performance; i.e., recovery of the velocity with least error. A large number of simulations were carried out with varying clutter filter width and window function (selected window function is the {von Hann}^{n}, and n varies), and the combination that resulted in the best performance (lowest *loss*, Sachidananda et al. 2000) is selected and listed in the tables. Tables 7.3a and 7.3b summarize the clutter filter performance, and also indicate the best combination of the clutter filter width, n_c, (n_c is the clutter filter width expressed as the number of deleted spectral coefficients) and the

exponent of the window function, {von Hann}^{n}, to be used for a given CSR. From the clutter map one could determine the value of n and n_c for each resolution cell, wherever clutter is to be filtered. The $sd(v)$ is computed only from correctly dealiased velocities. Note that the *loss* less than about 2% is mainly due to the velocity aliasing at the ends of the $\pm v_a$ interval, and is not due to the failure of the clutter filtering algorithm, hence can be ignored. It is seen from the Table 7.3 that the clutter filtering is good only up to CSR=30 dB for the 2.4° elevation. Beyond that the *loss* increases to about 9.4% for CSR =50 dB. The performance is similar for 5.35° also, because the PRT is nearly the same. It is obvious from the tables that for larger unambiguous velocity the performance improves because the "narrow" spectra criterion is satisfied better.

The simulation study indicates that if the CSR is large (>25 dB), a {von Hann}^{2} window is preferred, and for lower CSR (< 25 dB) the{von Hann} window performs better. Further, whenever a window weighting is applied, the samples at both ends of the time series are significantly attenuated. This loss of power increases the standard errors in the velocity estimate. To minimize this effect an extended time series can be used with zeros added at both ends, thus increasing the effective length of the sequence. With this extended time series, it is possible to keep the power loss due to windowing to approximately 3.5 dB, irrespective of which window is applied. For the {von Hann} window we can extend the time series length by about 14%, and for the {von Hann}^{2} window, the extension is about 32%. It is recommended that the extended time series processing be used whenever the window weighting is applied. Note that the pulse pair processing (no clutter, no overlay) gives the best estimates without the window. The overlay resolution algorithm requires {von Hann} window be applied to the time series. There is a special case of a very narrow width signal overlapping on a large clutter signal, discussed in Section 5 of this report, which can be resolved using a {von Hann}^{4} window. In this case the extended time series can be as long as 1.76 times the original series. Nonetheless, this situation is very rare.

Tables 7.4a and 7.4b are similar to the Tables 7.3a and 7.3b, but with the extended sample sequence. The time series is lengthened by adding zeros on both ends to the extent allowed by the window function. The parameter M^* is the length of the extended series. The extension is 14% (7% on each side) for {von Hann} window and 32% for the

{von Hann}^{2}. With this extended time series we can see a reduction in the standard error of all the spectral moment estimates, but there is an increase in the *loss* for large CSR. For CSR up to 30 dB, the extended series improves the standard errors, but for higher CSR the *loss* is larger although the standard errors are lower. Hence, it is recommended for lower CSR situations (<30 dB).

Tables 7.5a and 7.5b list the performance of the one-overlay resolution algorithm, applicable for only three elevations, 2.4°, 3.35°, and 4.3°. The first table is for w=3 m s^{-1}, and the next one is for w=4 m s^{-1}. In this simulation, the clutter is assumed to be absent, and p_1, p_2 are the signal powers of the overlaid echoes from the region-1 and region-3. The region-1 is 0 to $r_{a1}/2$, and the region-3 is r_{a1} to r_{a2}. The power p_2 is assumed to be higher, hence, the performance limit is indicated by the recovery of the weaker signal velocity, v_1, or the parameter $loss_1$. The algorithm can resolve velocities of both the overlaid signals, irrespective of whether p_1 or p_2 is stronger. If we take an upper limit of about 10% for the $loss_1$, from Table 7.5a we see that the overlay can be resolved up to p_2/p_1=30 dB for 2.4°, 40 dB for 3.35°, and more than 50 dB for 4.3° elevation. However, for larger signal spectrum width the performance deteriorates rapidly. For w=4 m s^{-1}, the overlay ratio limits are 9 dB, 15 dB, and about 33 dB for the three elevations. The reasons for this are well documented in Report 4.

8. Acknowledgements

This work is supported by the Radar Operations Center of NWS. The authors would like to thank Jim Evans of Lincoln Laboratory for suggesting to examine the possibility of using $R(T_1)$ for velocity estimation and $R(T_2)$ for dealiasing in the staggered PRT scheme.

9. Figures and Tables

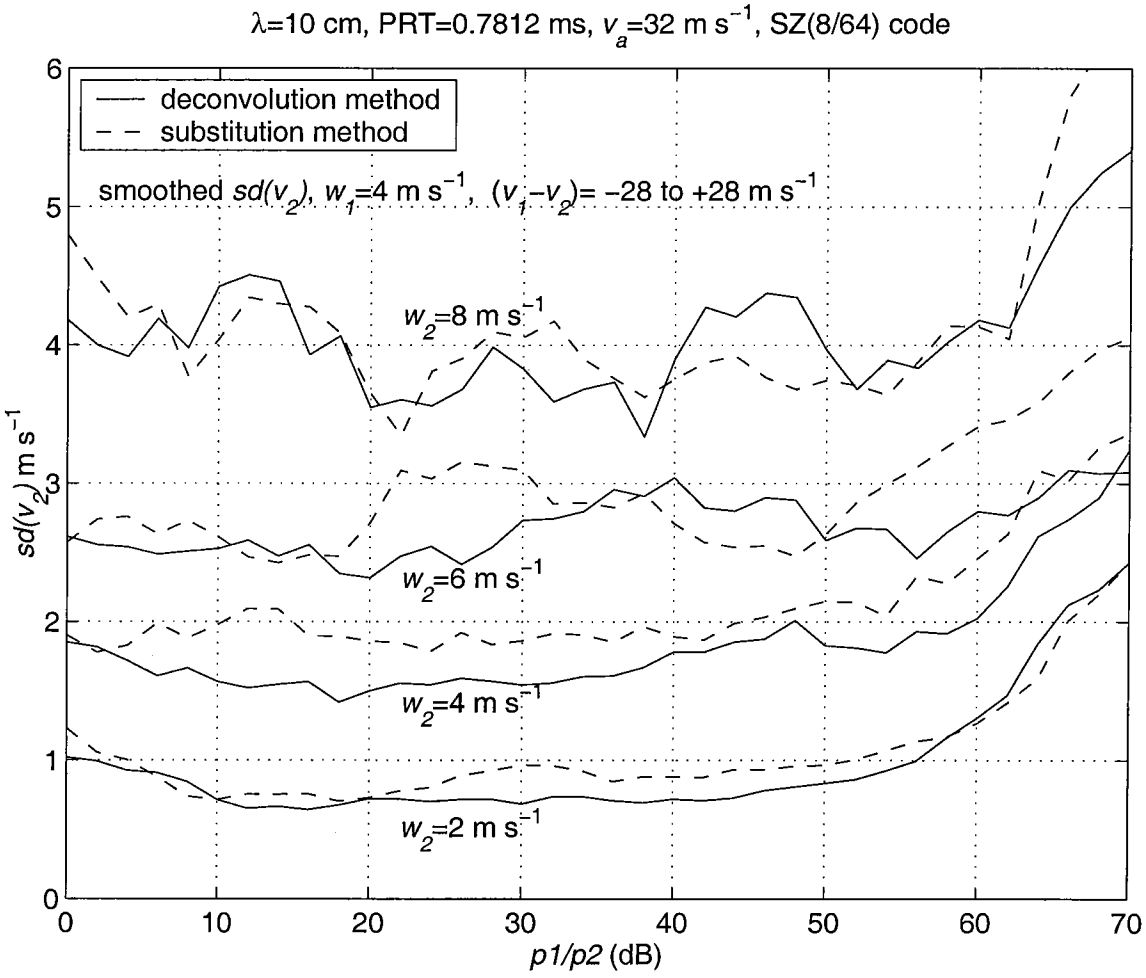

Fig.2.1. Comparison of the $sd(v)$ using the magnitude deconvolution and the substitution method.

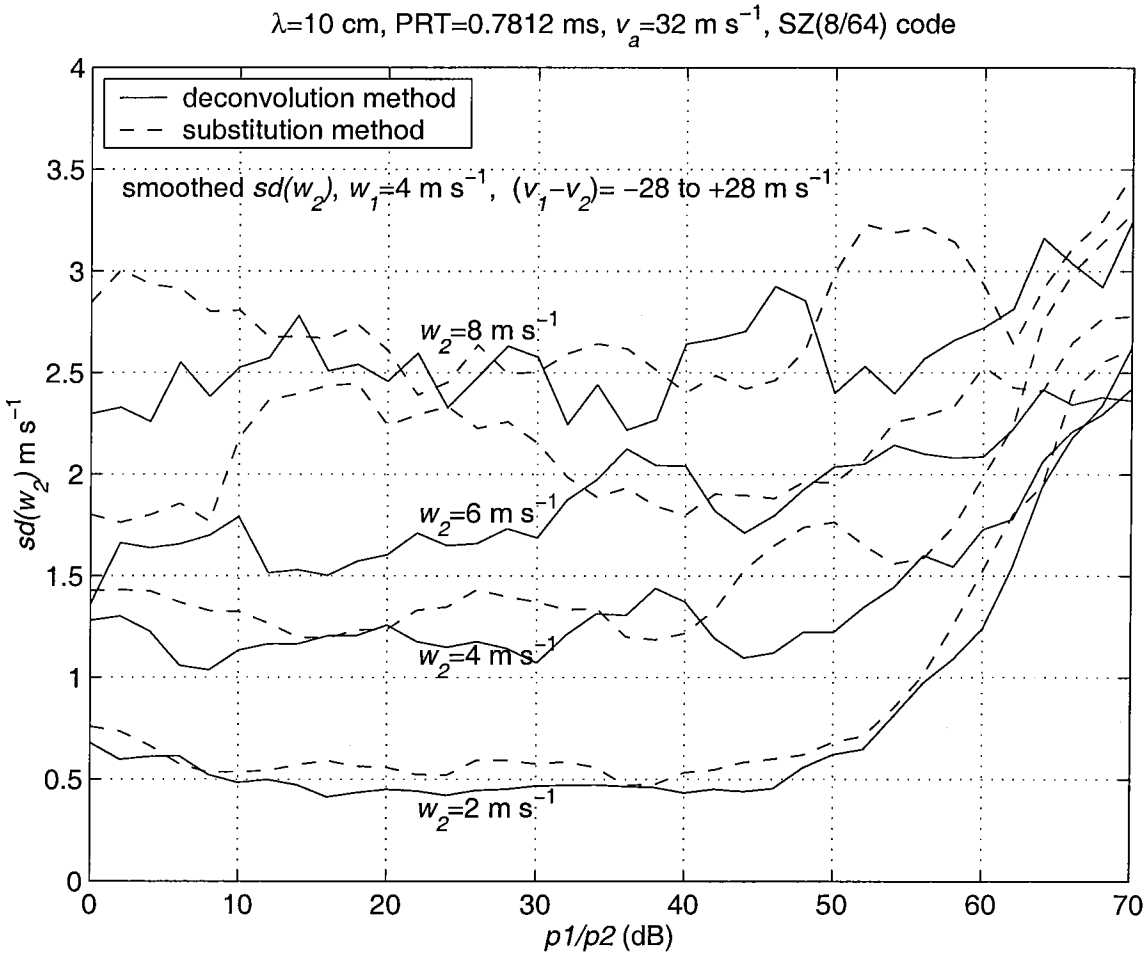

Fig. 2.2. Comparison of the *sd*(*w*) using the magnitude deconvolution and the substitution method.

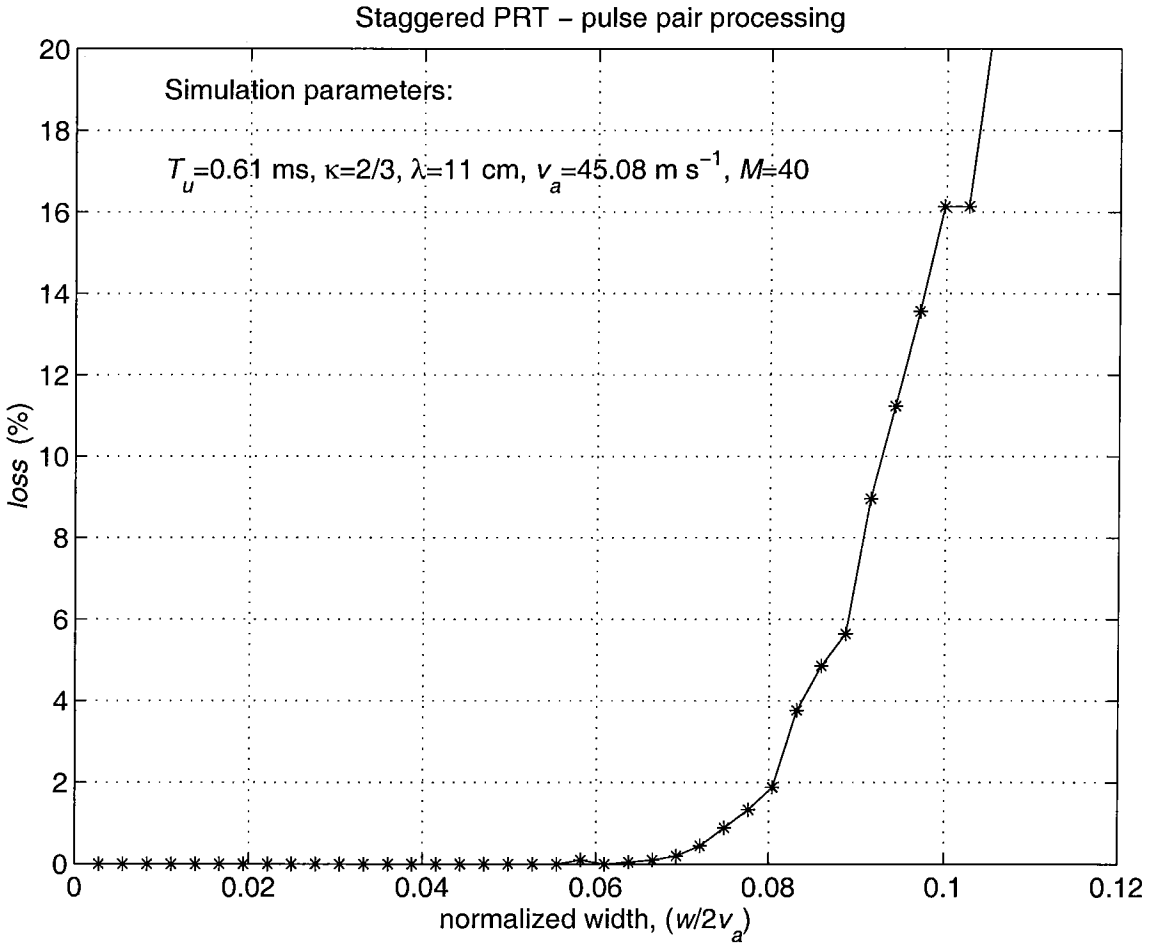

Fig. 3.1. The *% loss* versus the normalized spectrum width for the staggered PRT pulse pair processing method.

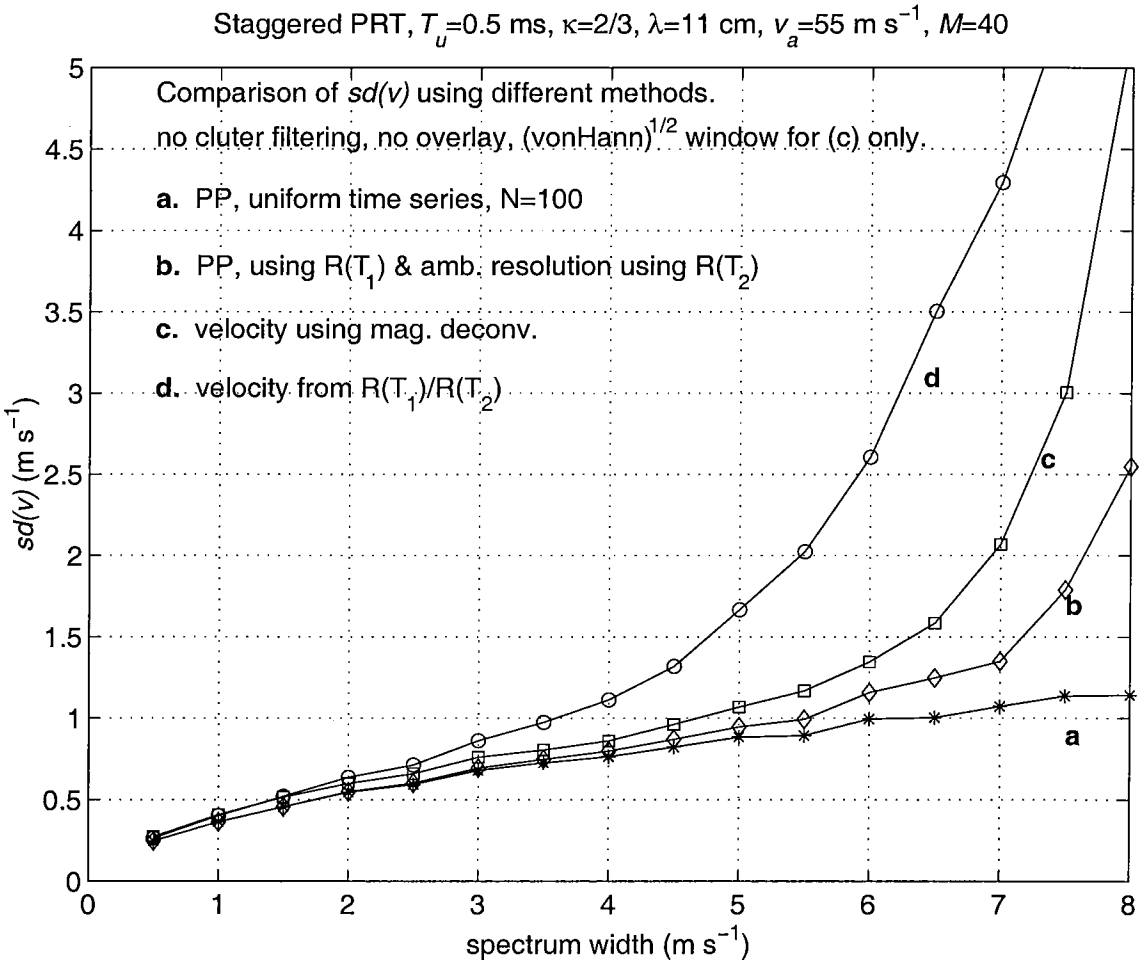

Fig. 3.2. A comparison of the *sd*(*v*) performance of different methods of staggered PRT processing.

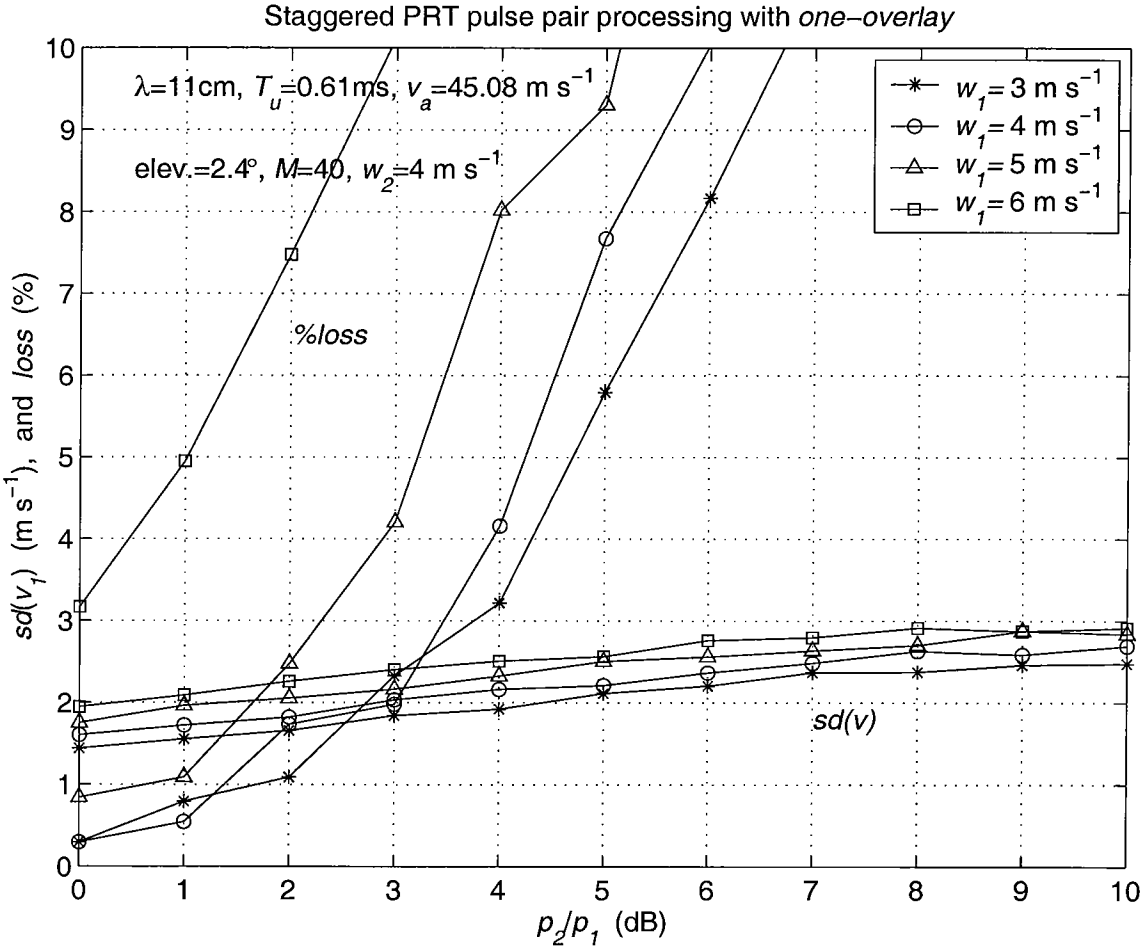

Fig. 3.3. The effect of one-overlay on the staggered PRT pulse pair algorithm; T_u=0.61ms.

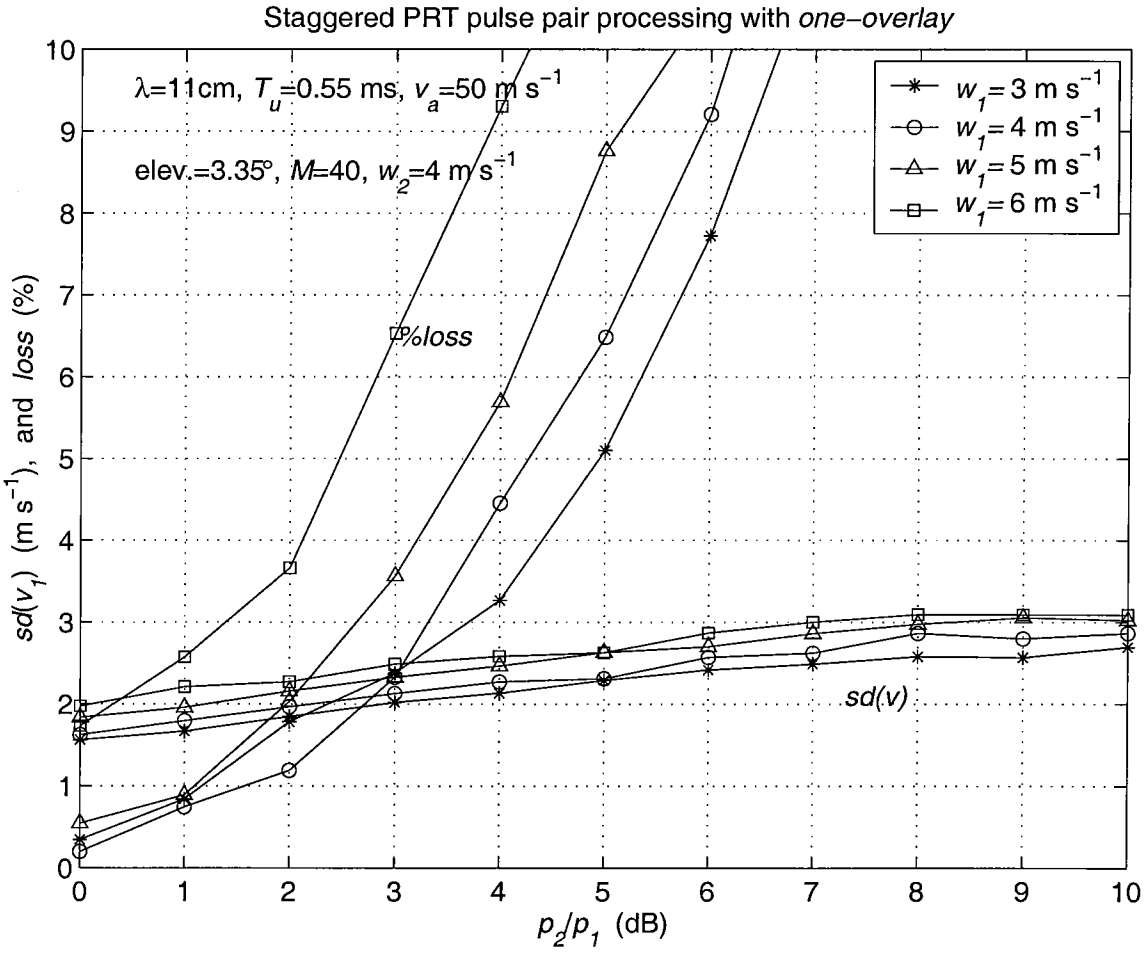

Fig. 3.4. The effect of one-overlay on the staggered PRT pulse pair algorithm; T_u=0.55ms.

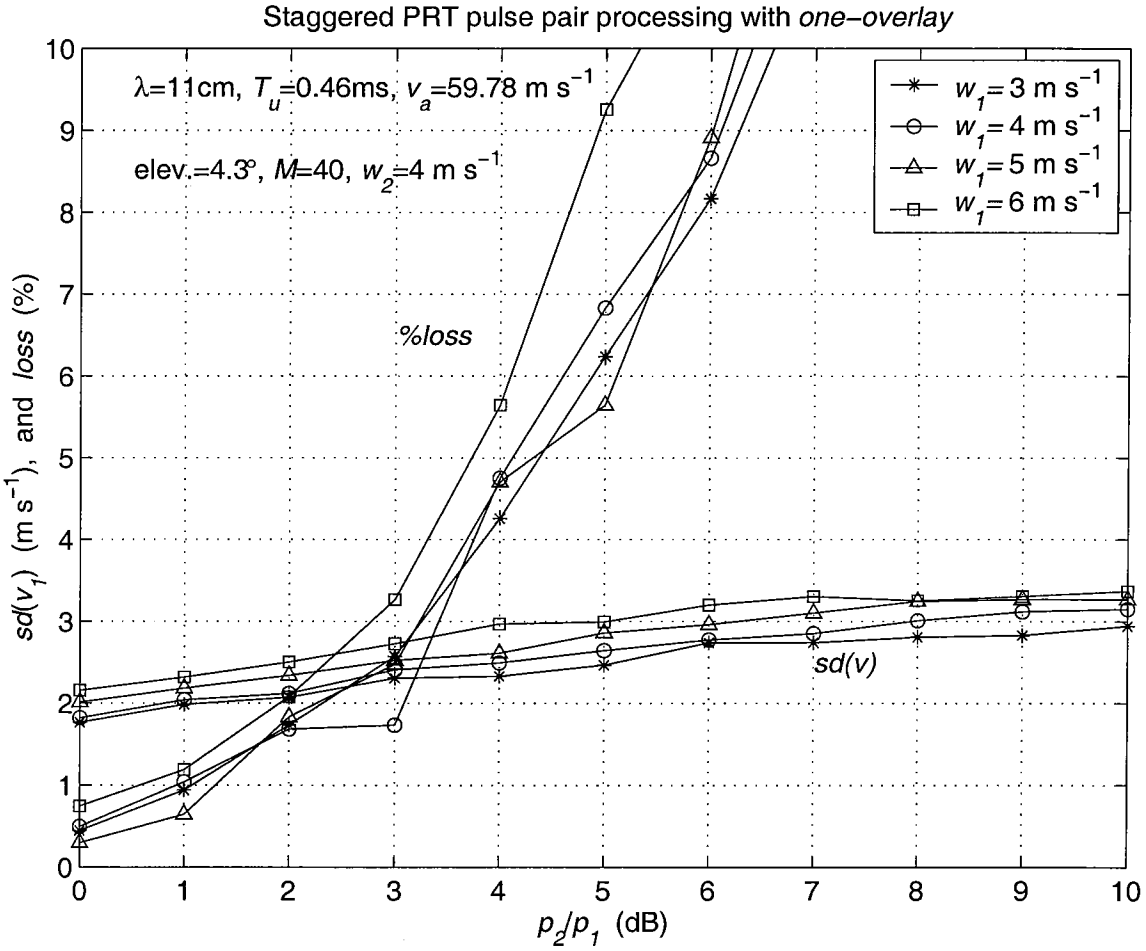

Fig. 3.5. The effect of one-overlay on the staggered PRT pulse pair algorithm; T_u=0.46ms.

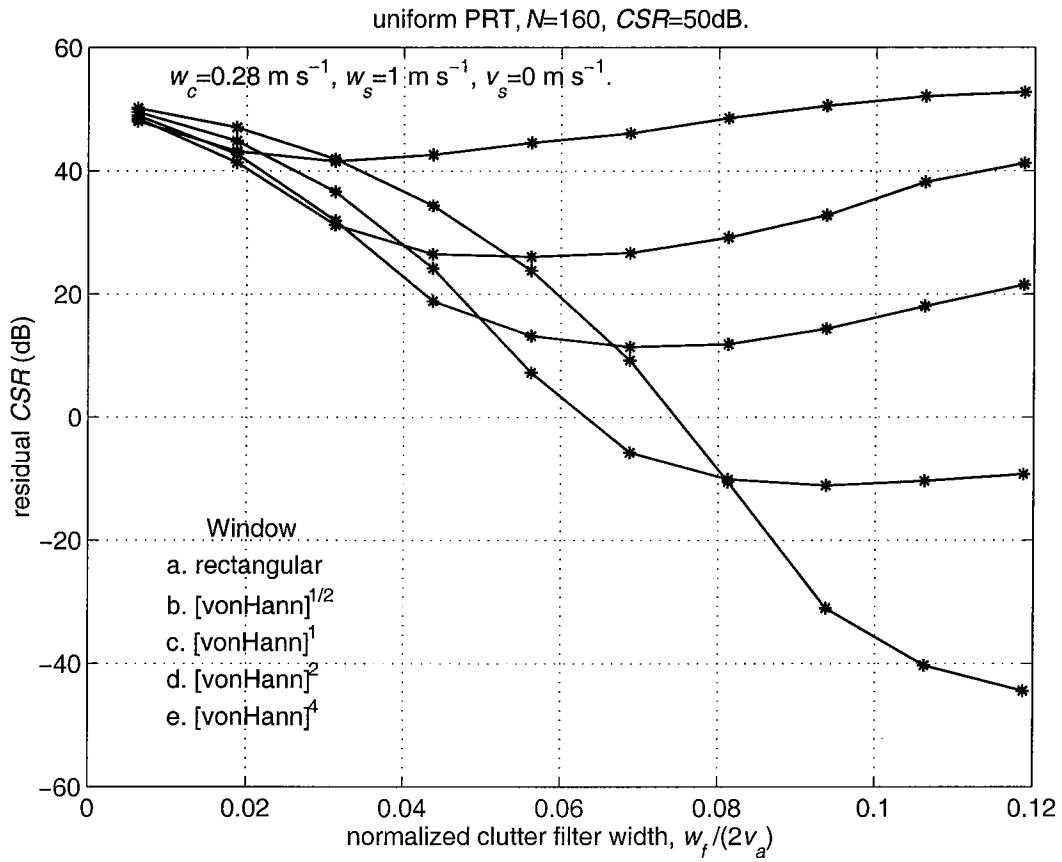

Fig. 5.1. The residual clutter-to-signal ratio (CSR) as a function of the normalized clutter filter width. Designation of window type from a to e, corresponds to the curves from top to bottom on the right side.

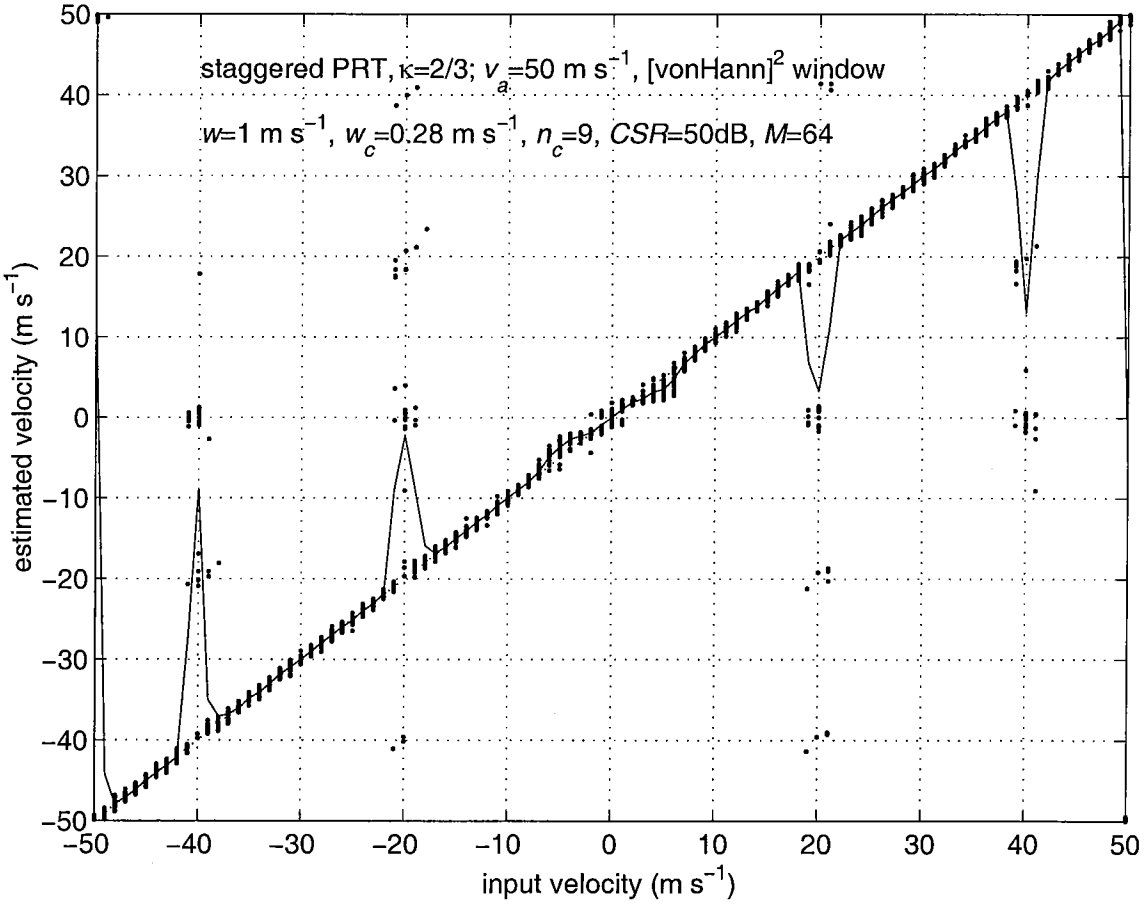

Fig. 5.2. The velocity recovery performance of the clutter filtering and the bias removal algorithm using the {von Hann}^{2} window.

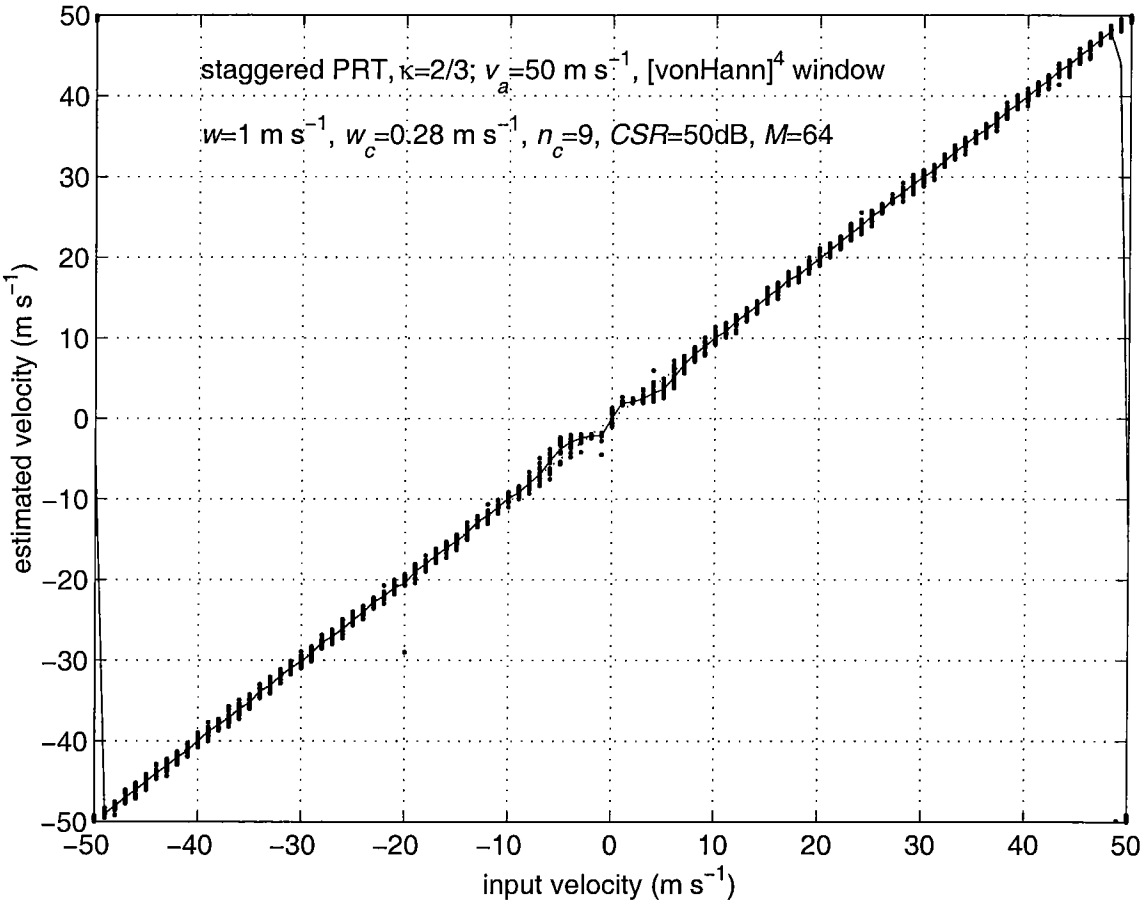

Fig. 5.3. The velocity recovery performance of the clutter filtering and the bias removal algorithm using the {von Hann}^{4} window. The simulation parameters are the same as in Fig. 5.2.

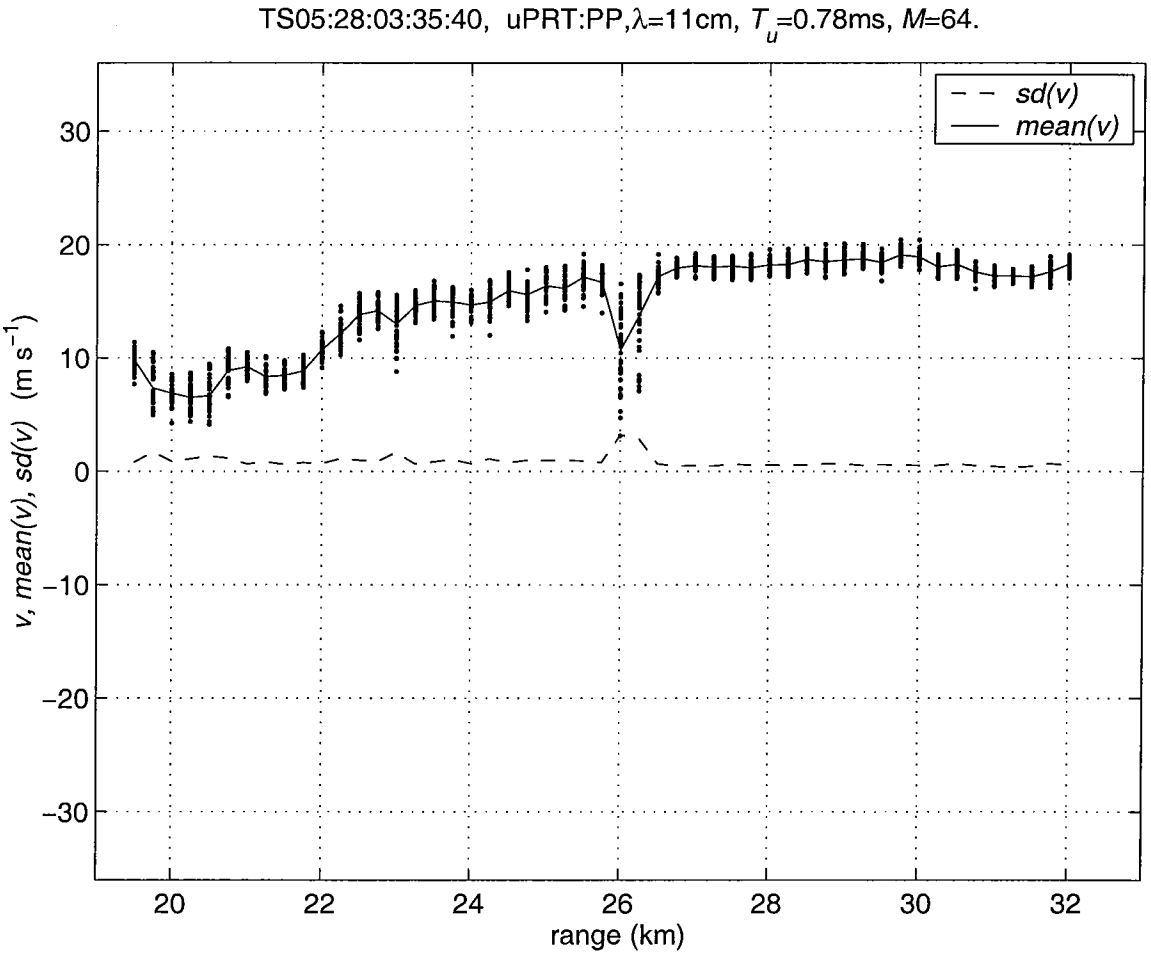

Fig. 6.1. A scatter plot of the velocity estimates using the uniform PRT sequence and the pulse pair algorithm. The time series data is described in case-1 of section-6. The mean and the standard deviation of the estimates are also shown.

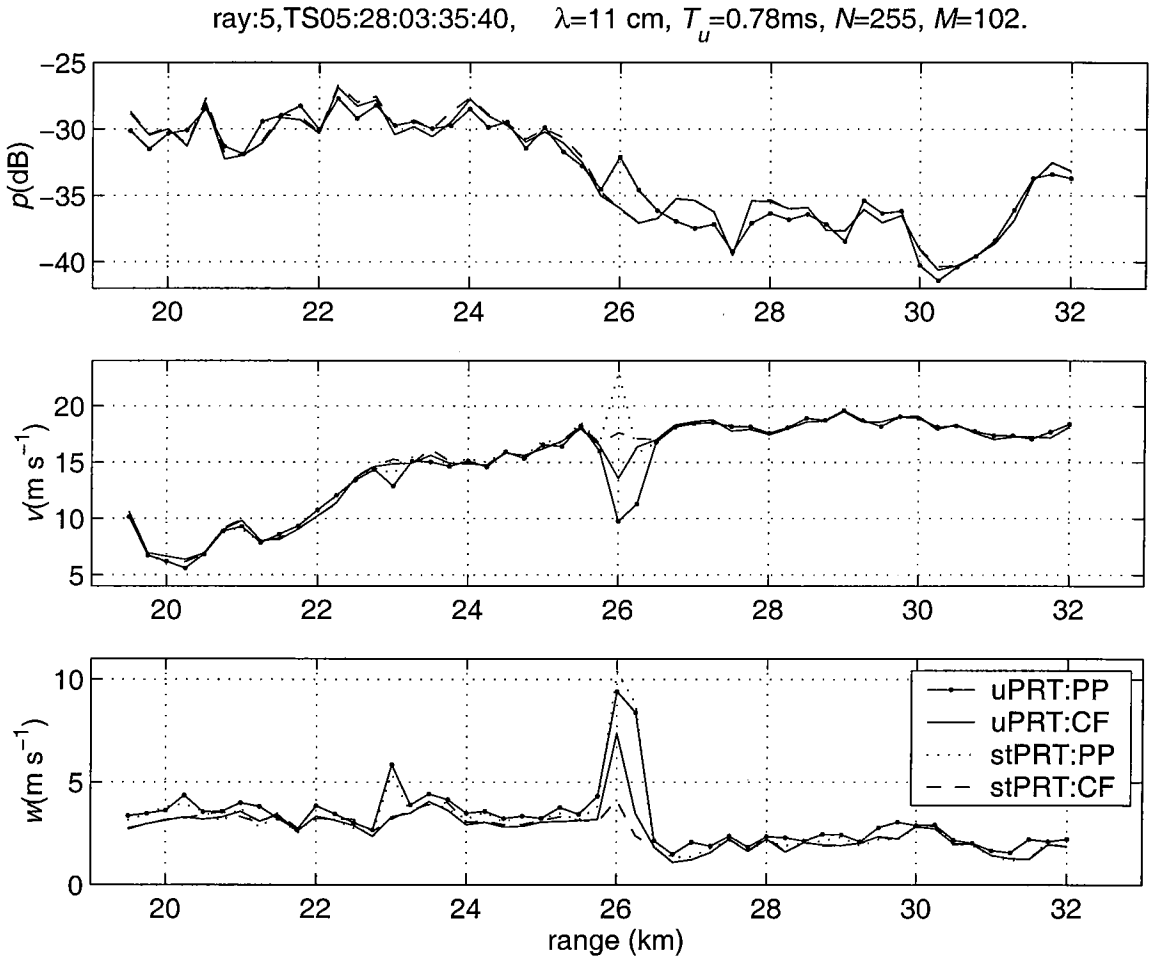

Fig. 6.2. The three spectral moments estimated using four different methods along one radial. The data is the same as in Fig. 6.1.

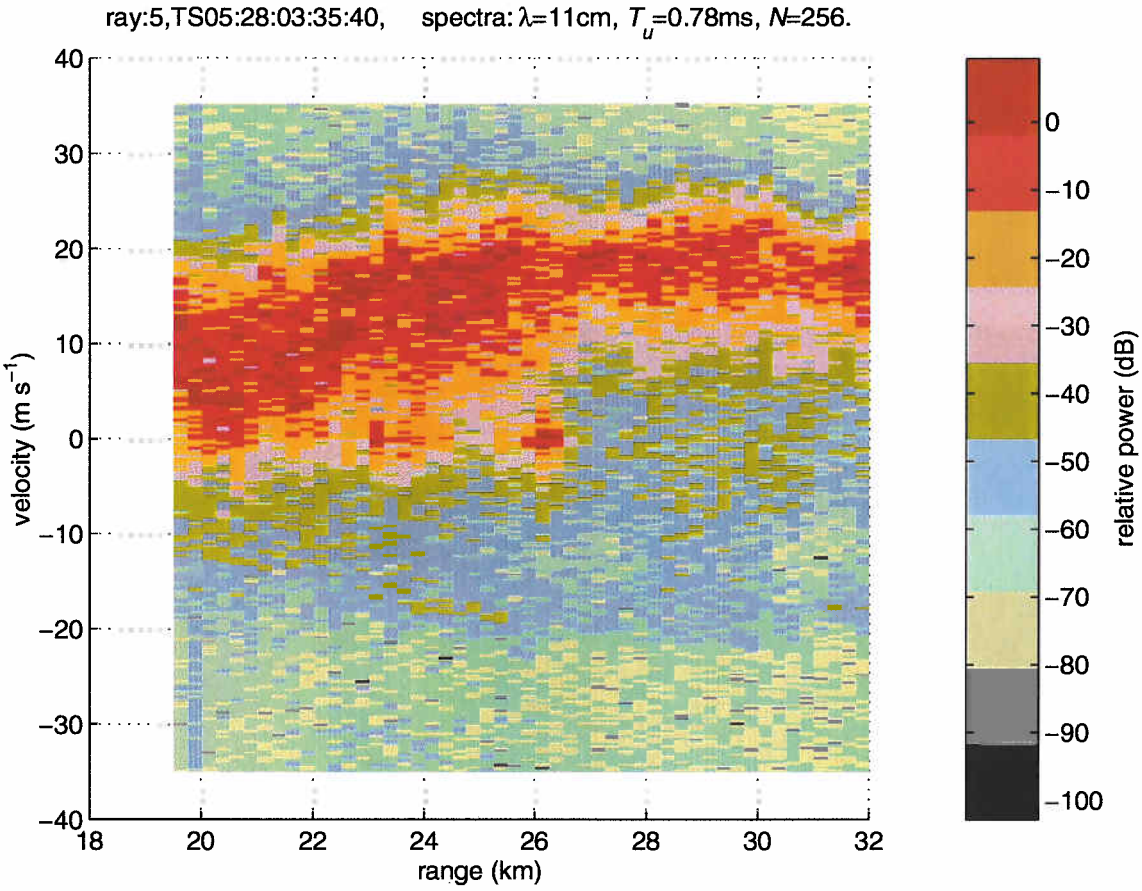

Fig. 6.3. The spectra along the same radial as in Fig. 6.2. The relative power scale is shown at the right.

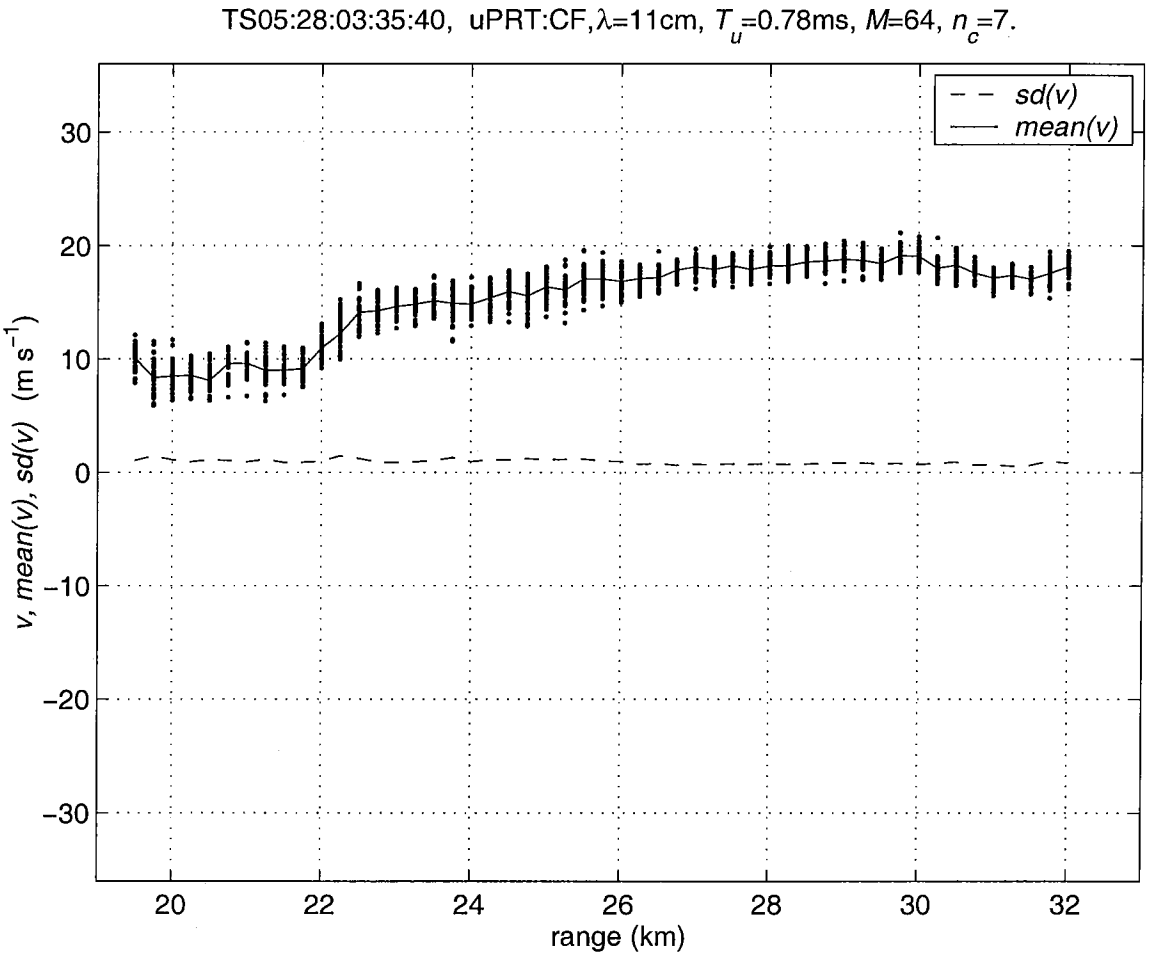

Fig. 6.4. A scatter plot of the velocity estimates using the uniform PRT sequence and the pulse pair algorithm after the clutter is filtered. The clutter is filtered in the spectral domain and the number of filter coefficients n_c=7. The data is the same as in Fig. 6.1.

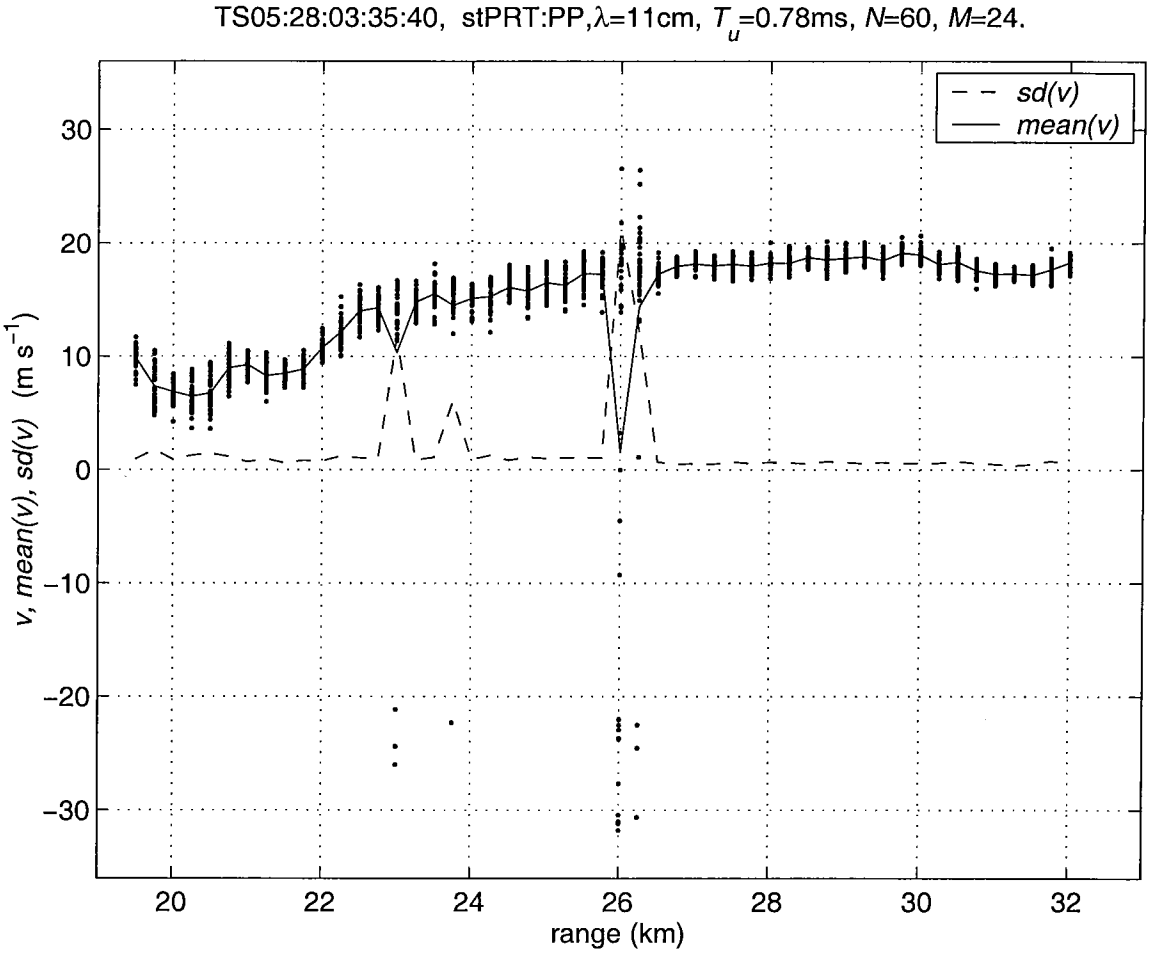

Fig. 6.5. The scatter plot of the velocity estimates from the derived time series processed using the staggered PRT pulse pair algorithm.

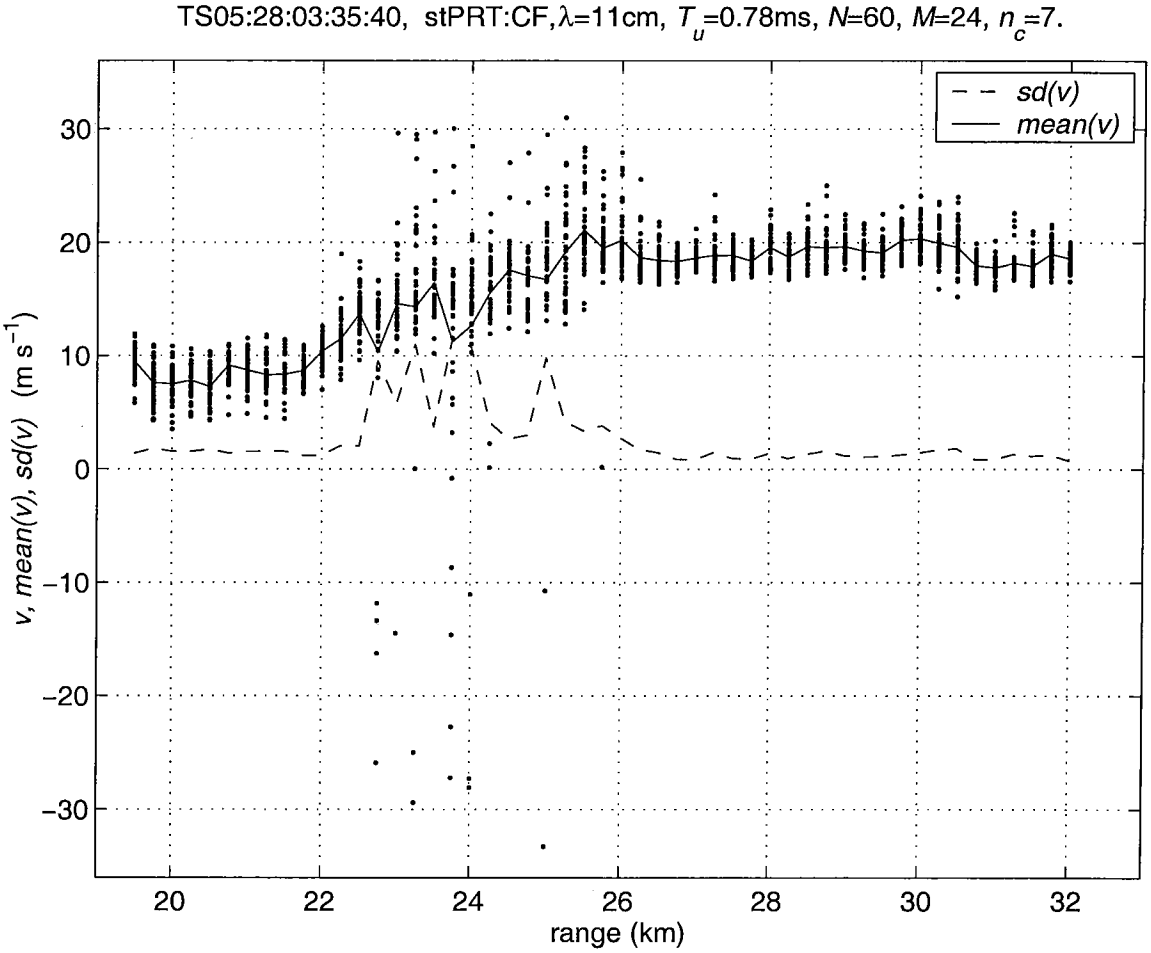

Fig. 6.6. The scatter plot of the velocity estimates for the same derived staggered PRT time series processed using the clutter filtering and bias removal algorithm.

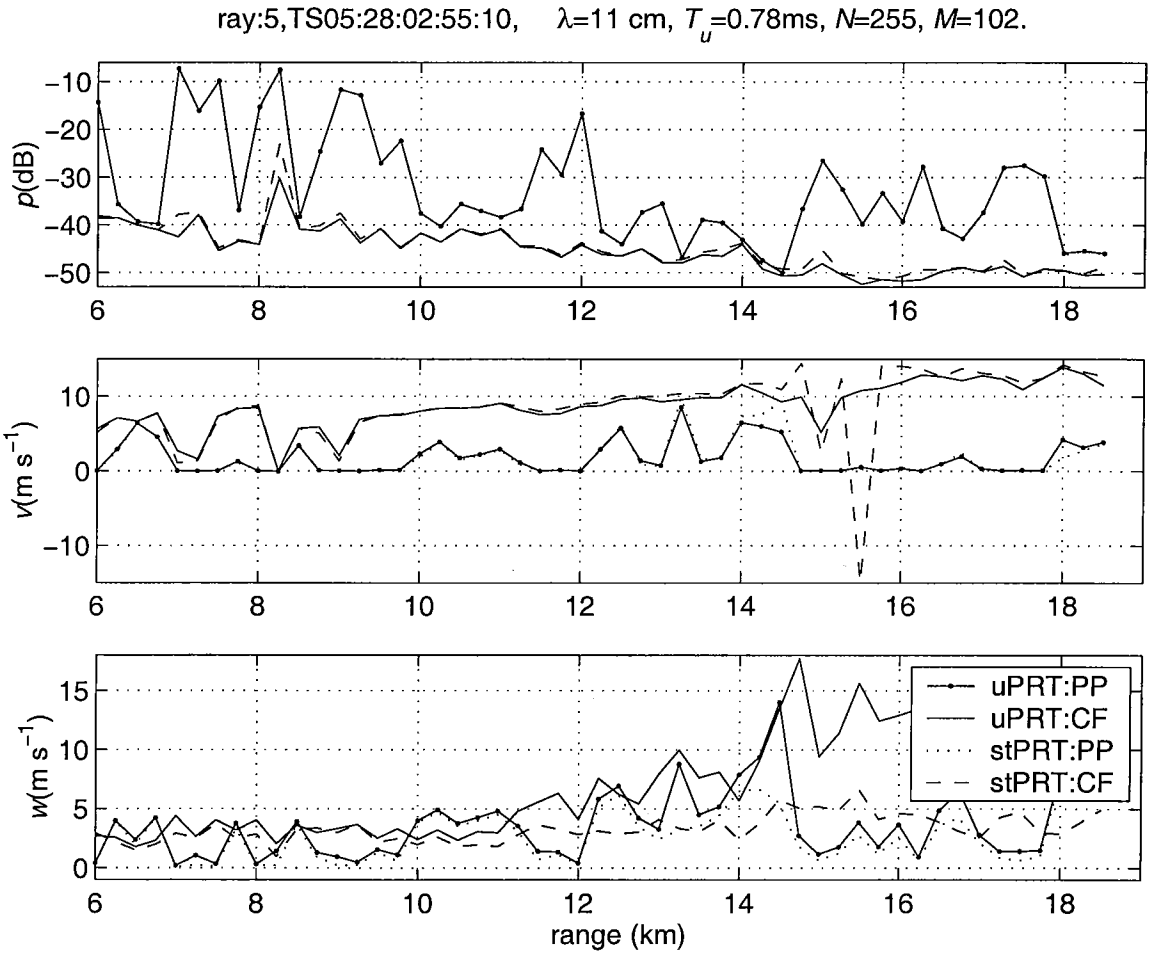

Fig. 6.7. The spectral moments for one radial of the data described in case-2 of section-6.

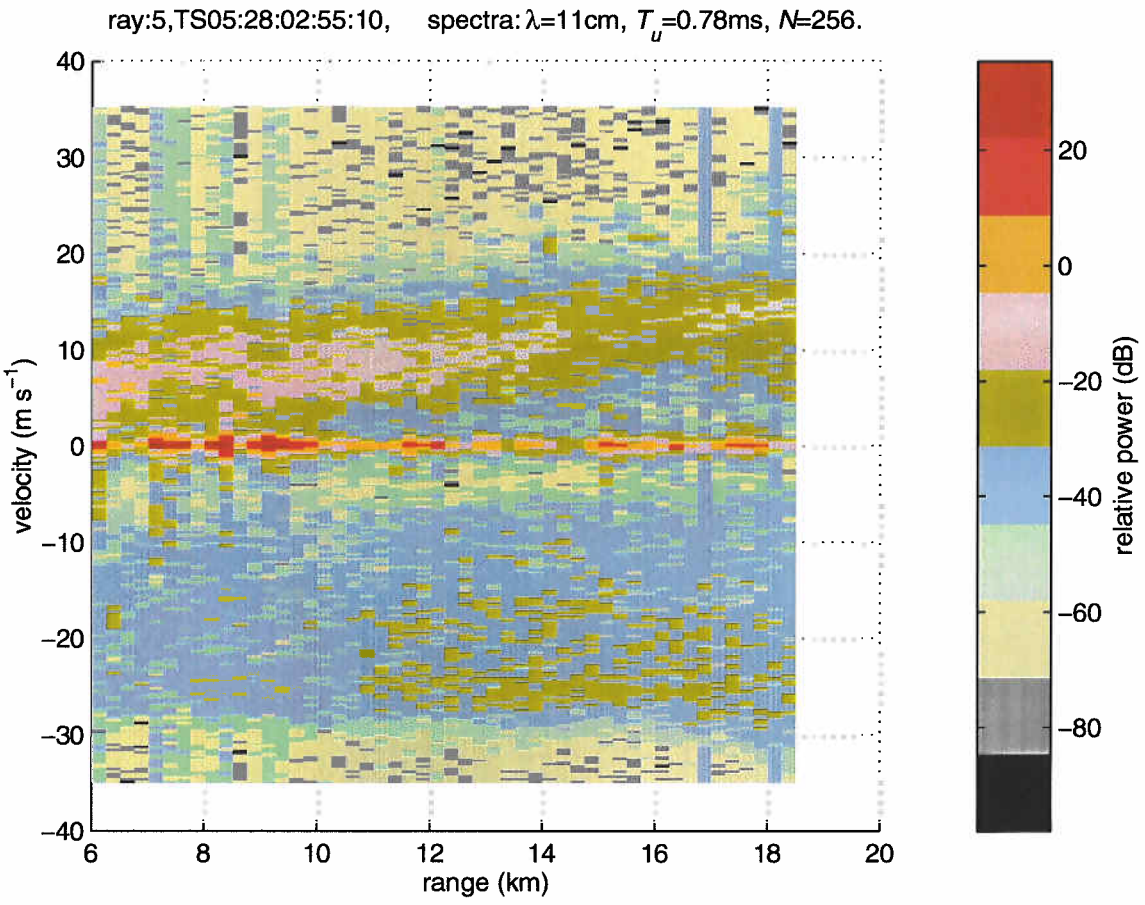

Fig. 6.8. The spectra along the same radial as in Fig. 6.7. The relative power scale is shown at the right.

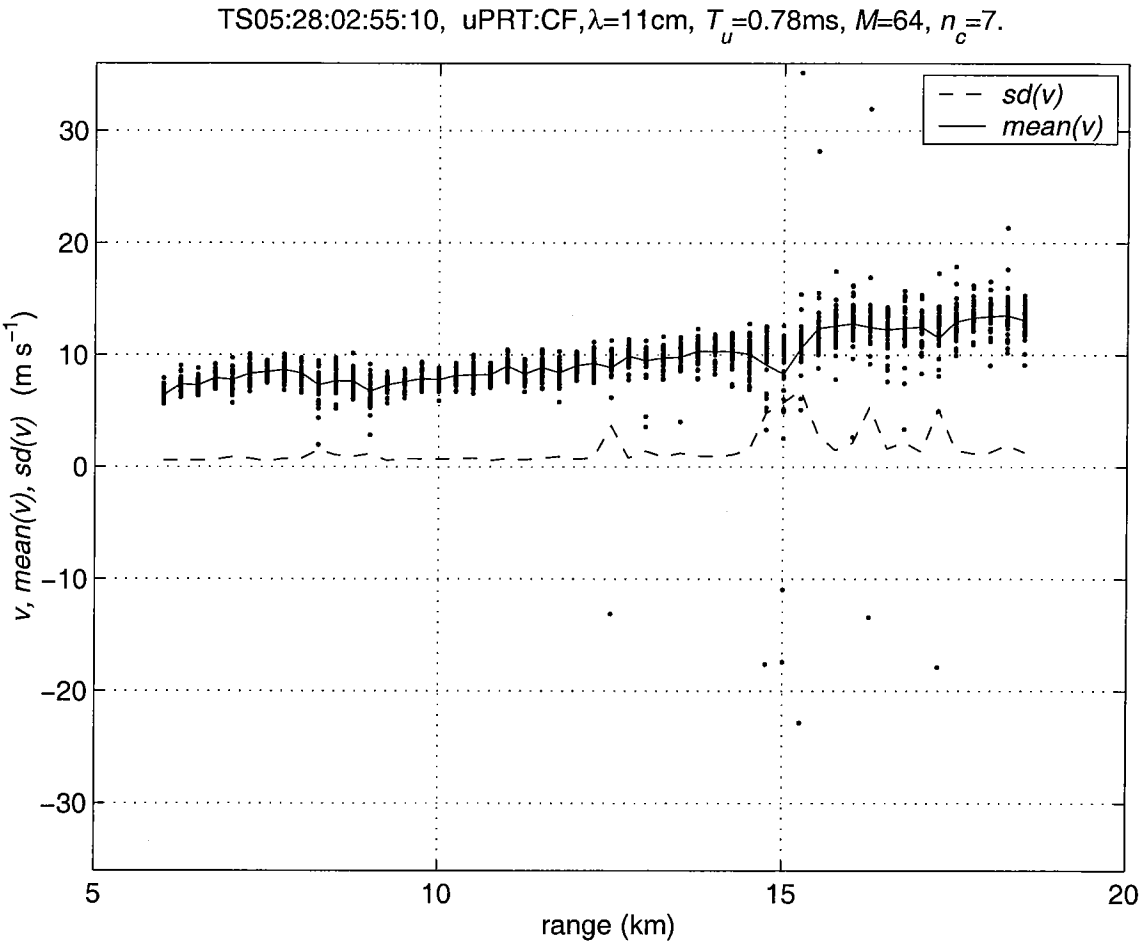

Fig. 6.9. The scatter plot of the velocity estimates form case-2 time series data, using the uniform PRT pulse pair algorithm applied after the clutter is filtered.

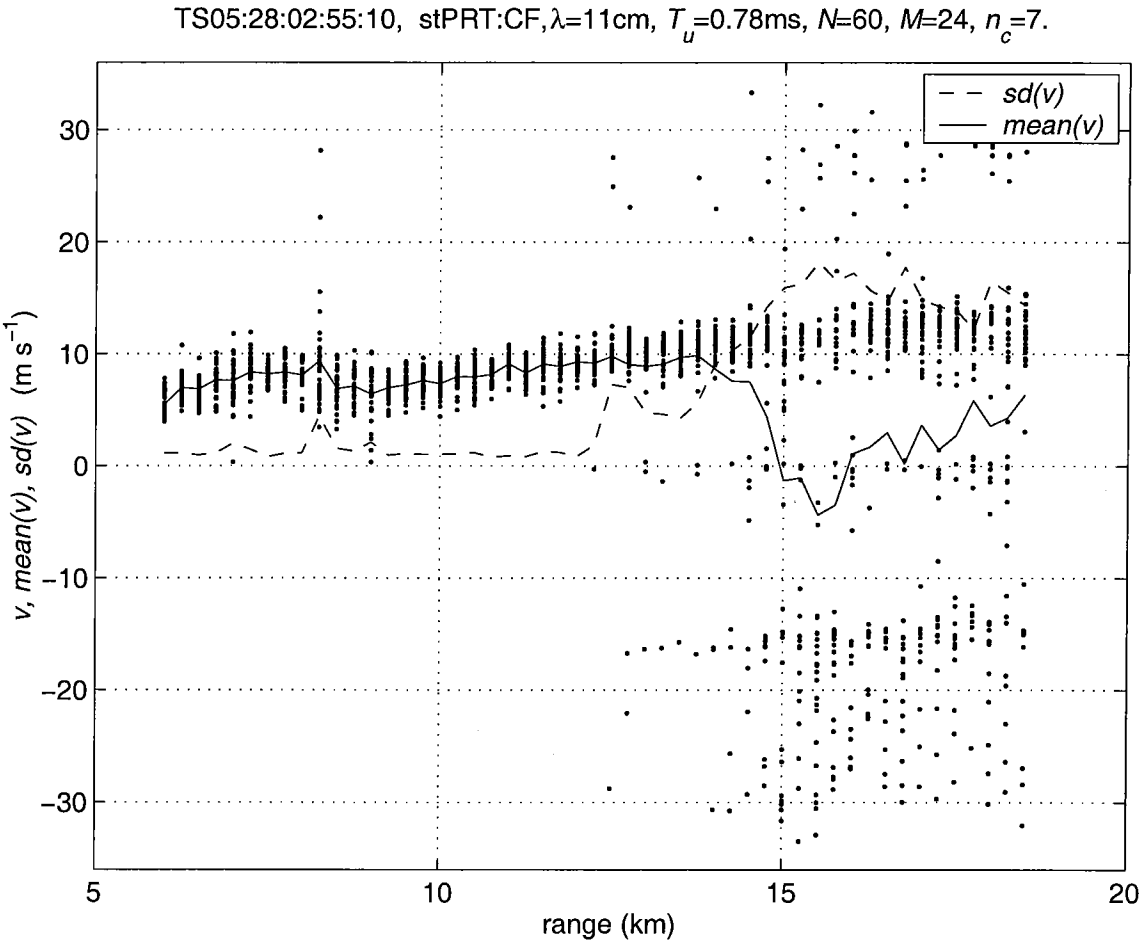

Fig. 6.10. The scatter plot of the velocity estimates form case-2 time series data, using the derived staggered PRT time series processed using the clutter filtering and bias removal algorithm.

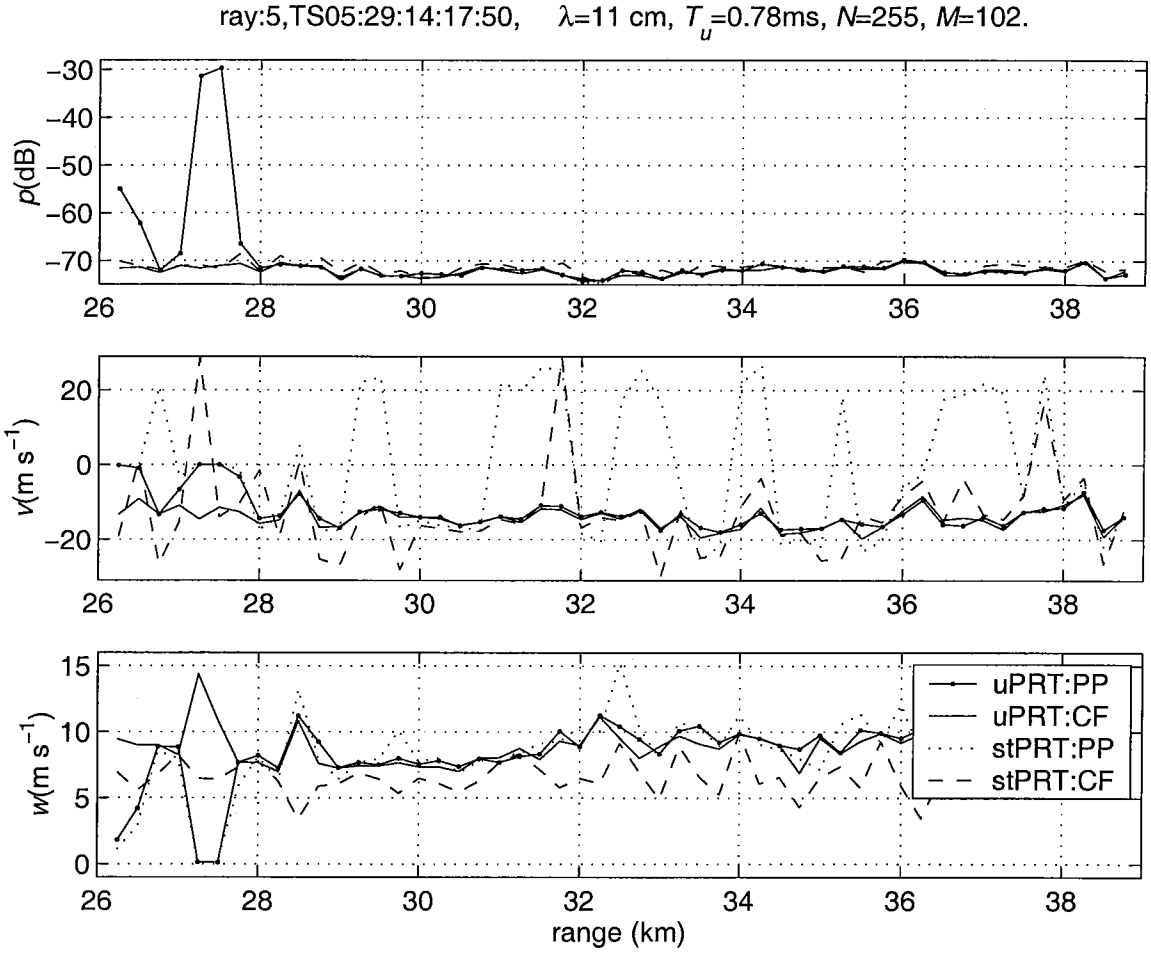

Fig. 6.11. The spectral moments for one radial of the data described in case-3 of section-6.

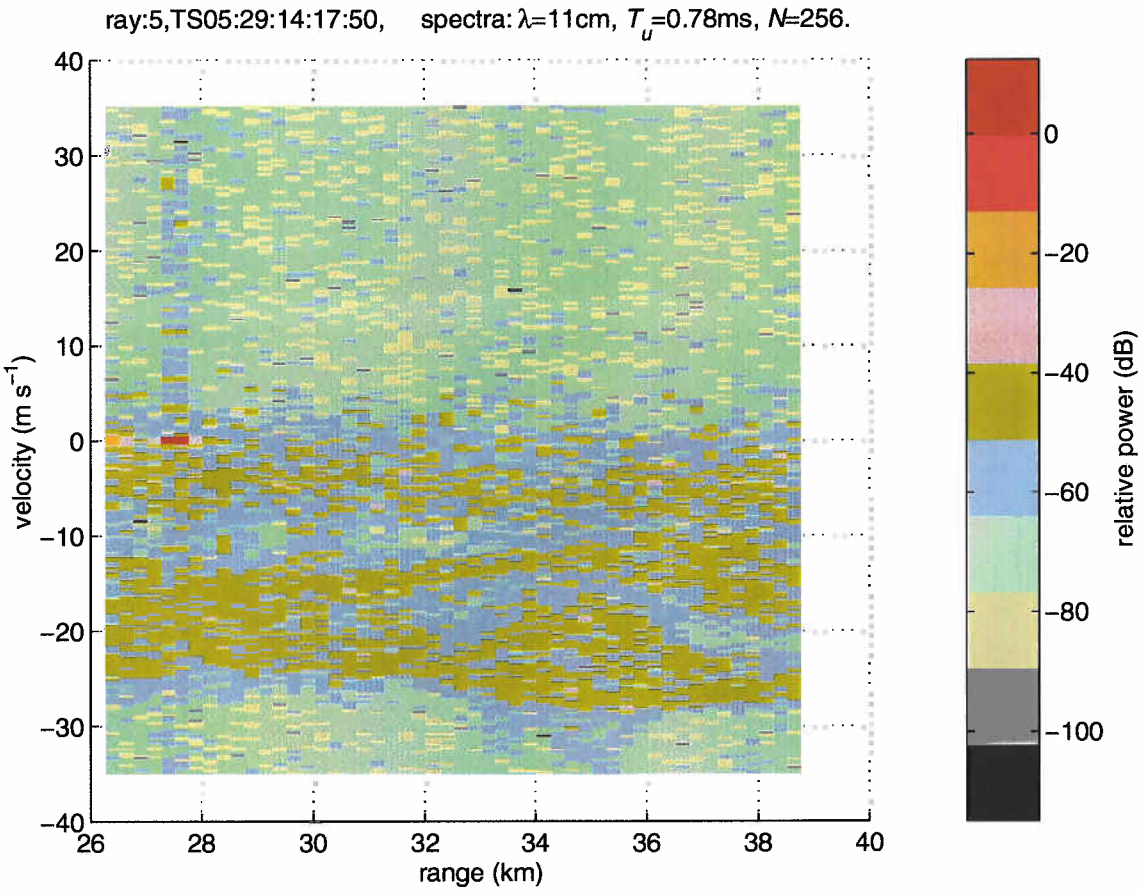

Fig. 6.12. The spectra along the same radial as in Fig. 6.11. The relative power scale is shown at the right.

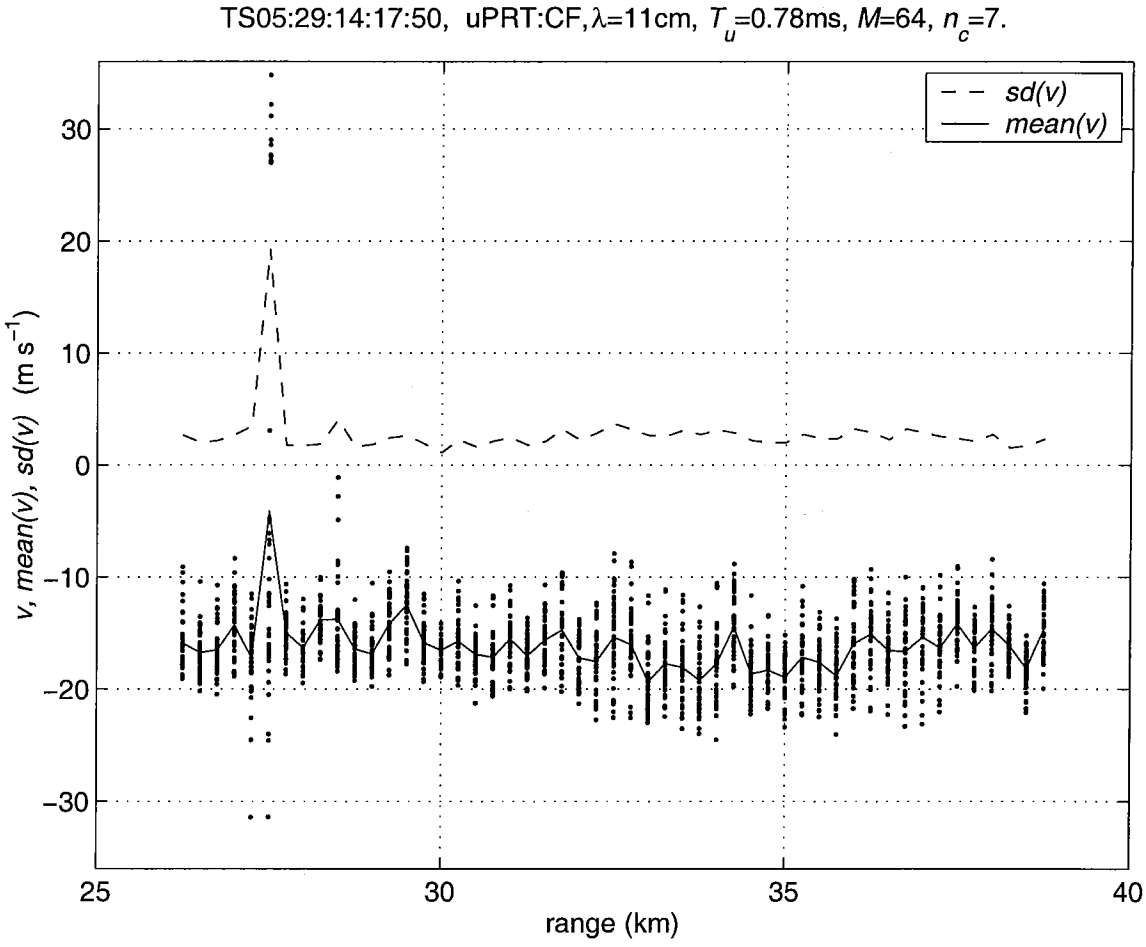

Fig. 6.13. The scatter plot of the velocity estimates form case-3 time series data, using the uniform PRT time series and the pulse pair algorithm. The clutter is filtered using a spectral domain filter before estimating the velocities.

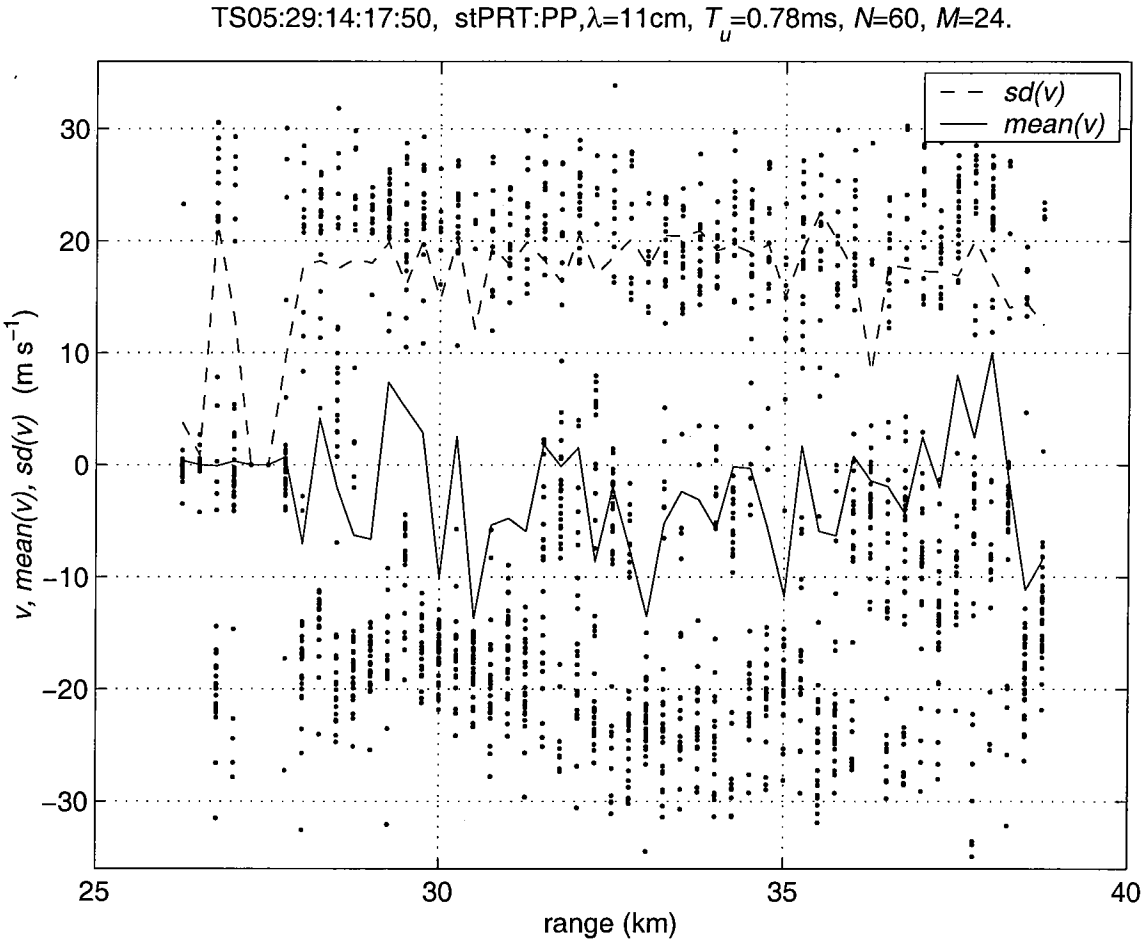

Fig. 6.14. The scatter plot of the velocity estimates form case-3 time series data, using the derived staggered PRT time series and the pulse pair algorithm. The clutter is not filtered.

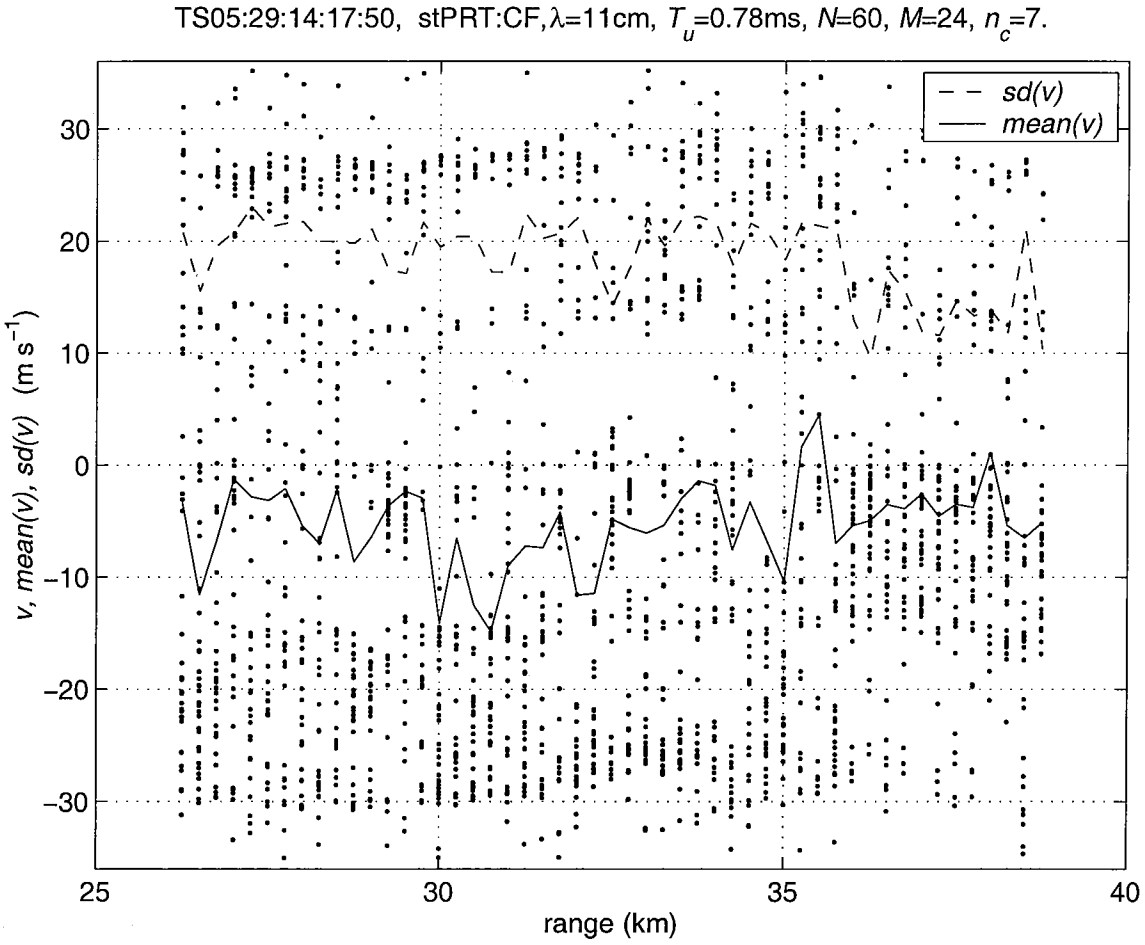

Fig. 6.15. The scatter plot of the velocity estimates from time series data of case-3; the derived staggered PRT time series is processed using the clutter filtering and bias removal algorithm.

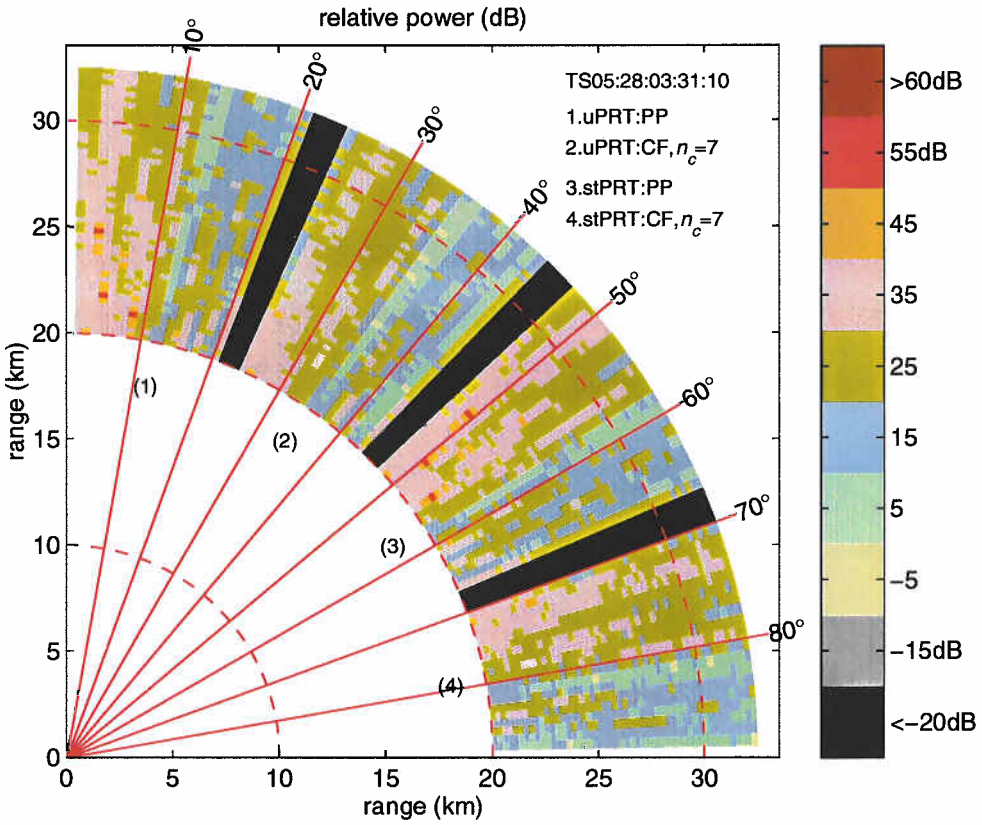

Fig. 6.16. The PPI display of the mean power estimate in relative power units (in dB), using four different algorithms indicated in the legend. The data is described in case-4 of the section-6.

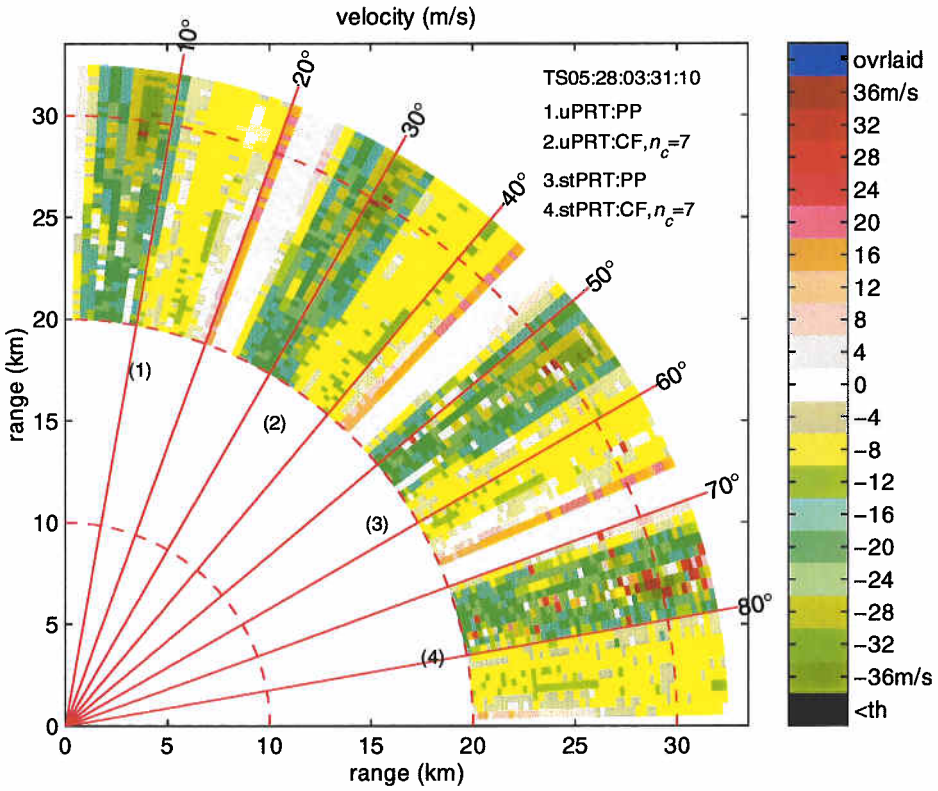

Fig. 6.17. The PPI display of the mean velocity estimate using four different algorithms indicated in the legend. The time series data is the same as in Fig. 6.16.

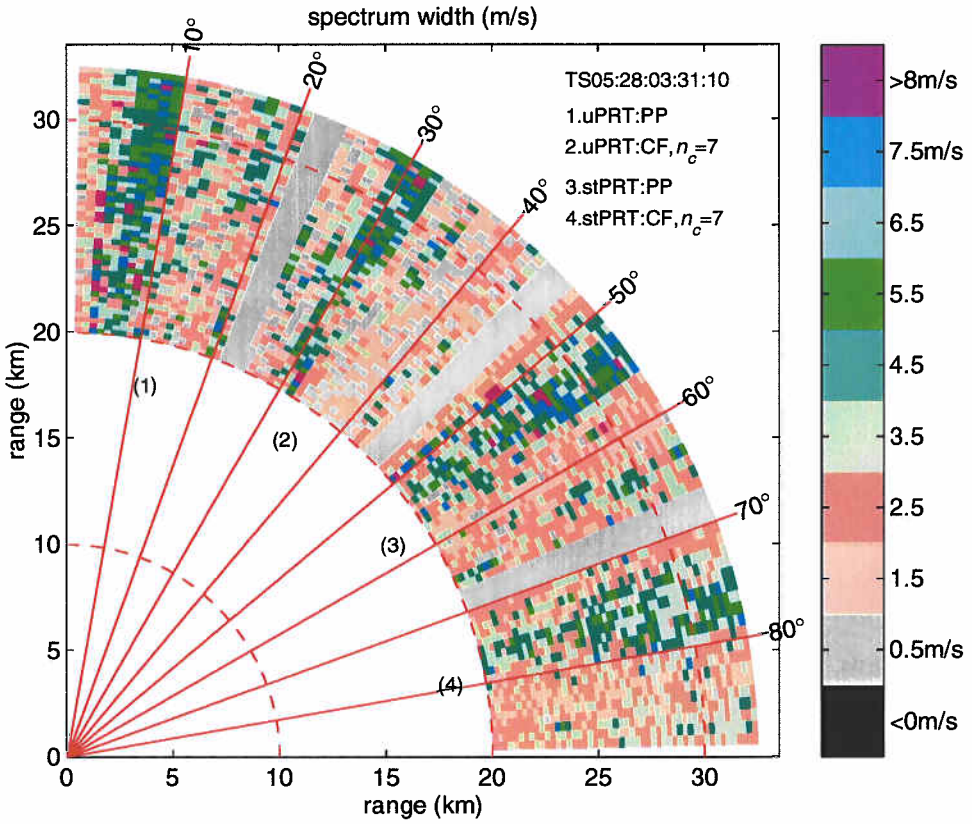

Fig. 6.18. The PPI display of the spectrum width estimate using four different algorithms indicated in the legend. The time series data is the same as in Fig. 6.16.

Table. 7.1a. A proposed volume coverage pattern for the WSR-88D (revised).

Elev.	AZ rate (°/sec)	period (sec.)	dwell time (ms)	WF[(1)] type	T_u (ms)	T_1 (ms)	T_2 (ms)	M	r_{max} (km)	r_{a1} (km)	r_{a2} (km)	v_a (m/s)
0.5°	18.7	19.38	48.45	CS,1	3.11	-	-	17	460	466	-	-
0.5°	19.2	18.83	47.08	SZ(8/64)	0.78	-	-	52	460	234	-	35.3
1.45°	19.8	18.24	45.60	CS,1	3.11	-	-	16	379	466	-	-
1.45°	19.2	18.83	47.08	SZ(8/64)	0.78	-	-	52	379	234	-	35.3
2.4°	16.1	22.46	56.15	STO(2/3)	0.61	1.22	1.83	37	303	183	275	45.1
3.35°	17.9	20.23	50.58	STO(2/3)	0.55	1.1	1.65	37	247	165	248	50.0
4.3°	17.9	20.23	50.58	STO(2/3)	0.46	0.92	1.38	44	207	138	207	59.8
5.25°	17.5	20.73	51.83	ST(2/3)	0.59	1.18	1.77	35	177	177	-	46.6
6.2°	17.5	20.73	51.83	ST(2/3)	0.51	1.02	1.53	41	154	153	-	53.9
7.5°	25.2	14.38	35.95	ST(2/3)	0.44	0.88	1.32	33	131	132	-	62.5
8.7°	25.4	14.25	35.63	ST(2/3)	0.38	0.76	1.14	38	115	114	-	72.4
10°	25.4	14.24	35.60	ST(2/3)	0.36	0.72	1.08	40	100	108	-	76.4
12°	25.5	14.22	35.55	ST(2/3)	0.36	0.72	1.08	40	85	108	-	76.4
14°	25.5	14.19	35.48	ST(2/3)	0.36	0.72	1.08	39	73	108	-	76.4
16.7°	25.6	14.14	35.35	ST(2/3)	0.36	0.72	1.08	39	62	108	-	76.4
19.5°	25.7	14.09	35.23	ST(2/3)	0.36	0.72	1.08	39	54	108	-	76.4

[(1)] Abbreviations: WF - Waveform.
CS,1 - Contiguous surveillance (same as the original WSR-88D scheme), PRF #1.
SZ(*n/M*) - SZ phase coded contiguous Doppler.
STO(κ) - Staggered PRT with one-overlay resolution algorithm.
ST(κ) - Staggered PRT, no overlay resolution.

Table. 7.1b. A proposed volume coverage pattern for the WSR-88D (Table 7.1 continued).
(standard errors in the spectral parameter estimates)

Elev.	WF type	T_u (ms)	M [3]	[2]standard errors, $w=w_2=2$ m s^{-1},$w_1=4$ m s^{-1}			[2]standard errors, $w=w_1=w_2=4$ m s^{-1}			[2]standard errors, $w=w_2=6$ m s^{-1},$w_1=4$m s^{-1}		
				sd(p) dB	*sd(v)* m s^{-1}	*sd(w)* m s^{-1}	*sd(p)* dB	*sd(v)* m s^{-1}	*sd(w)* m s^{-1}	*sd(p)* dB	*sd(v)* m s^{-1}	*sd(w)* m s^{-1}
0.5°	CS,1	3.11	17	1.64	-	-	1.12	-	-	1.05	-	-
0.5°	SZ(8/64)	0.78	52	1.96, 2.66	1.30, 1.04	0.95, 1.32	1.76, 1.99	1.38, 1.67	1.00, 1.84	1.78, 2.41	1.32, 2.94	0.90, 2.64
1.45°	CS,1	3.11	16	1.81	-	-	1.2	-	-	1.08	-	-
1.45°	SZ(8/64)	0.78	52	1.96, 2.66	1.30, 1.04	0.95, 1.32	1.76, 1.99	1.38, 1.67	1.00, 1.84	1.78, 2.41	1.32, 2.94	0.90, 2.64
2.4°	STO(2/3)	0.61	38	1.60	0.52	0.33	1.08	0.78	0.56	0.90	1.44	0.96
3.35°	STO(2/3)	0.55	36	1.66	0.54	0.35	1.14	0.84	0.54	0.99	1.36	1.01
4.3°	STO(2/3)	0.46	44	1.65	0.53	0.33	1.18	0.78	0.49	0.97	1.07	0.84
5.25°	ST(2/3)	0.59	34	1.63	0.53	0.33	1.20	0.84	0.59	0.98	1.52	1.08
6.2°	ST(2/3)	0.51	40	1.68	0.55	0.34	1.14	0.80	0.50	0.98	1.13	0.92
7.5°	ST(2/3)	0.44	32	1.95	0.63	0.40	1.39	0.92	0.58	1.16	1.26	0.93
8.7°	ST(2/3)	0.38	38	1.96	0.64	0.40	1.39	0.93	0.59	1.15	1.19	0.82
10°	ST(2/3)	0.36	40	2.03	0.62	0.40	1.41	0.93	0.57	1.13	1.18	0.82
12°	ST(2/3)	0.36	40	2.03	0.62	0.40	1.41	0.93	0.57	1.13	1.18	0.82
14°	ST(2/3)	0.36	40	2.03	0.62	0.40	1.41	0.93	0.57	1.13	1.18	0.82
16.7°	ST(2/3)	0.36	40	2.03	0.62	0.40	1.41	0.93	0.57	1.13	1.18	0.82
19.5°	ST(2/3)	0.36	40	2.03	0.62	0.40	1.41	0.93	0.57	1.13	1.18	0.82

[2] The two standard errors in each column are for the stronger and weaker signals in the scheme with SZ(8/64) code; the w_1, w_2 correspond to the spectrum width of signals in the 1st and 2nd trip and the overlay ratio is $p1/p2$=20 dB. For the staggered PRT {STO(2/3) and ST(2/3)}, the numbers refer to the pulse pair algorithm with no clutter and no overlay and the spectrum width is w.
[3] The number of samples M used in the simulation is rounded off to the nearest even integer for the staggered PRT processing.

Table. 7.2. The standard errors in the spectral parameter estimates using staggered PRT and pulse pair algorithm for different PRT selections.

Elev.	range r_{a1},r_{a2} (km)	T_u (ms)	M	standard errors, w=2 m s^{-1}			standard errors, w=4 m s^{-1}			standard errors, w=6 m s^{-1}		
				sd(p) dB	*sd(v)* m s^{-1}	*sd(w)* m s^{-1}	*sd(p)* dB	*sd(v)* m s^{-1}	*sd(w)* m s^{-1}	*sd(p)* dB	*sd(v)* m s^{-1}	*sd(w)* m s^{-1}
2.4°	183, 275	0.61	38	1.60	0.52	0.33	1.08	0.78	0.56	0.90	1.44	0.96
2.4°	204, 306	0.68	32	1.63	0.52	0.33	1.18	0.93	0.64	0.95	1.35, 5.2%	1.09
2.4°	234, 351	0.78	30	1.58	0.52	0.32	1.12	0.88	0.74	0.92	1.48, 12%	1.17
2.4°	300, 450	1.00	22	1.55	0.55	0.36	1.12	1.16, 7.5%	0.92	0.99	1.54, 38%	1.40
3.35°	150, 225	0.50	40	1.71	0.54	0.34	1.18	0.84	0.51	0.98	1.13	0.93
3.35°	165, 248	0.55	36	1.66	0.54	0.35	1.14	0.84	0.54	0.99	1.36	1.01
3.35°	180, 270	0.60	34	1.65	0.54	0.35	1.16	0.85	0.58	0.98	1.61	1.05
3.35°	210, 315	0.70	28	1.75	0.57	0.34	1.16	0.92	0.74	1.01	1.50, 6%	1.20
3.35°	246, 369	0.82	24	1.66	0.54	0.34	1.19	1.21	0.77	0.99	1.56, 18%	1.36
4.3°	138, 207	0.46	44	1.65	0.53	0.33	1.18	0.78	0.49	0.97	1.07	0.84
4.3°	150, 225	0.50	40	1.68	0.54	0.34	1.14	0.80	0.51	0.99	1.15	0.92
4.3°	165, 248	0.55	36	1.66	0.55	0.35	1.20	0.80	0.56	0.93	1.17	1.01
4.3°	180, 270	0.60	34	1.66	0.54	0.32	1.15	0.81	0.58	0.96	1.40	1.07
4.3°	207, 311	0.69	28	1.70	0.55	0.35	1.20	0.88	0.71	1.03	1.42, 4.6%	1.19
5.25°	177	0.59	34	1.63	0.53	0.33	1.20	0.84	0.59	0.98	1.52	1.08
6.2°	153	0.51	40	1.68	0.55	0.34	1.14	0.80	0.50	0.98	1.13	0.92
7.5°	132	0.44	32	1.95	0.63	0.40	1.39	0.92	0.58	1.16	1.26	0.93
8.7°	114	0.38	38	1.96	0.64	0.40	1.39	0.93	0.59	1.15	1.19	0.82
10°	108	0.36	40	2.03	0.62	0.40	1.41	0.93	0.57	1.13	1.18	0.82

Note: M is rounded off to the nearest even number for the staggered PRT processing. The second number in the *sd(v)* column is the percentage *loss*, indicated only when it is significant. The unresolved velocities are not included in the *sd(v)* calculation. For elevations higher than 10° the values are the same as that in the last row, since the PRTs are the same.

Table. 7.3a. The staggered PRT clutter filtering performance for CSR=20 dB and 30 dB, w=4 m s^{-1}.

elev. (deg.)	2.4°	3.35°	4.3°	5.25°	6.2°	7.5°	8.7°	10°
T_u (ms)	0.61	0.55	0.46	0.59	0.51	0.44	0.38	0.36
M	36	36	44	34	40	32	38	40
CSR (dB)	20	20	20	20	20	20	20	20
n_c	7	7	7	7	7	7	7	7
n in {vH}^{n}	1	1	1	2	1	1	1	1
$sd(p)$ (dB)	1.76	1.74	1.72	1.92	1.69	2.09	2.13	2.04
$sd(v)$ (m s^{-1})	1.40	1.31	1.20	1.54	1.24	1.40	1.40	1.32
$sd(w)$ (m s^{-1})	0.76	0.74	0.70	0.83	0.72	0.85	0.81	0.77
loss (%)	1.98%	1.24%	0.59%	1.83%	0.59%	0.94%	0.45%	0.45%
CSR (dB)	30	30	30	30	30	30	30	30
n_c	7	7	9	7	7	7	7	7
n in {vH}^{n}	2	2	2	2	2	2	2	2
$sd(p)$ (dB)	1.93	1.99	2.04	2.01	1.97	2.40	2.30	2.28
$sd(v)$ (m s^{-1})	1.52	1.55	1.42	1.47	1.42	1.57	1.51	1.54
$sd(w)$ (m s^{-1})	0.82	0.83	0.82	0.85	0.77	0.94	0.87	0.87
loss (%)	2.87%	1.98%	0.54%	3.22%	0.74%	1.58%	0.64%	0.64%

Note: *loss* is the number of times the velocity is not resolved correctly as a percentage of the total number of simulations (about 2000). *loss* < 2% is generally observed to be because of the velocity folding at the ends of the Nyquist interval, $\pm v_a$. The n_c and n, the exponent of {von Hann}^{n} is the optimum for the CSR (and the clutter width, w_c=0.28 m s^{-1}). The shaded part is for CSR=20dB, and the unshaded last 7 rows are for CSR=30 dB.

Table. 7.3b. The staggered PRT clutter filtering performance for CSR=40 dB and 50 dB, w=4 m s^{-1}.

elev. (deg.)	2.4°	3.35°	4.3°	5.25°	6.2°	7.5°	8.7°	10°
T_u (ms)	0.61	0.55	0.46	0.59	0.51	0.44	0.38	0.36
M	36	36	44	34	40	32	38	40
CSR (dB)	40	40	40	40	40	40	40	40
n_c	7	9	9	7	9	9	9	7
n in $\{vH\}^n$	2	2	2	2	2	2	2	2
$sd(p)$ (dB)	1.95	2.12	2.01	1.96	2.04	2.45	2.42	2.26
$sd(v)$ (m s^{-1})	1.59	1.50	1.37	1.56	1.51	1.62	1.59	1.56
$sd(w)$ (m s^{-1})	0.95	0.86	0.79	0.94	0.84	0.98	0.93	1.12
loss (%)	5.25%	3.26%	0.74%	6.24%	1.83%	3.32%	1.04%	0.99%
CSR (dB)	50	50	50	50	50	50	50	50
n_c	9	9	11	9	11	9	11	9
n in $\{vH\}^n$	2	2	2	2	2	2	2	2
$sd(p)$ (dB)	2.03	2.11	2.14	2.17	2.11	2.48	2.46	2.36
$sd(v)$ (m s^{-1})	1.60	1.62	1.47	1.62	1.47	1.62	1.55	1.58
$sd(w)$ (m s^{-1})	0.95	0.99	0.89	1.02	0.88	1.20	1.06	1.19
loss (%)	9.41%	6.73%	2.28%	9.70%	3.76%	6.73%	3.17%	1.88%

Note: *loss* is the number of times the velocity is not resolved correctly as a percentage of the total number of simulations (about 2000). *loss* < 2% is generally observed to be because of the velocity folding at the ends of the Nyquist interval, $\pm v_a$. The n_c and n, the exponent of {von Hann}^{n} is the optimum for the CSR (and the clutter width, w_c=0.28 m s^{-1}). The shaded part is for CSR=40dB, and the unshaded last 7 rows are for CSR=50 dB.

Table. 7.4a. The staggered PRT clutter filtering performance for CSR=20 dB and 30 dB, w=4 m s^{-1}, using the extended time series.

elev. (deg.)	2.4°	3.35°	4.3°	5.25°	6.2°	7.5°	8.7°	10°
T_u (ms)	0.61	0.55	0.46	0.59	0.51	0.44	0.38	0.36
CSR (dB)	20	20	20	20	20	20	20	20
M*	40	44	50	44	44	42	42	44
n_c	7	7	7	7	7	7	7	7
n in {vH}^{n}	1	1	1	2	1	2	1	1
sd(p) (dB)	1.54	1.59	1.60	1.72	1.58	2.01	1.99	1.87
sd(v) (m s^{-1})	1.23	1.19	1.10	1.32	1.21	1.39	1.34	1.32
sd(w) (m s^{-1})	0.71	0.75	0.72	0.73	0.73	0.78	0.87	0.85
loss (%)	1.24%	0.49%	0.15%	1.14%	0.35%	0.50%	0.30%	0.24%
CSR (dB)	30	30	30	30	30	30	30	30
M*	46	52	58	44	52	42	50	52
n_c	7	7	7	7	7	7	7	7
n in {vH}^{n}	2	2	2	2	2	2	2	2
sd(p) (dB)	1.61	1.63	1.61	1.69	1.63	1.93	1.84	1.91
sd(v) (m s^{-1})	1.3	1.25	1.20	1.33	1.29	1.42	1.41	1.38
sd(w) (m s^{-1})	0.74	0.92	0.87	0.77	0.88	0.92	1.36	1.39
loss (%)	1.14%	0.79%	0.24%	1.29%	0.40%	0.89%	0.79%	0.64%

Note: M* is the extended time series length. *loss* is the number of times the velocity is not resolved correctly as a percentage of the total number of simulations (about 2000). *loss* < 2% is generally observed to be because of the velocity folding at the ends of the Nyquist interval, $\pm v_a$. The n_c and n, the exponent of {von Hann}^{n} is the optimum for the CSR (and the clutter width, w_c=0.28 m s^{-1}). The shaded part is for CSR=20dB, and the unshaded last 8 rows are for CSR=30 dB.

Table. 7.4b. The staggered PRT clutter filtering performance for CSR=40 dB and 50 dB, w=4 m s^{-1}, using the extended time series.

elev. (deg.)	2.4°	3.35°	4.3°	5.25°	6.2°	7.5°	8.7°	10°
T_u (ms)	0.61	0.55	0.46	0.59	0.51	0.44	0.38	0.36
CSR (dB)	40	40	40	40	40	40	40	40
M^*	46	52	58	44	52	42	50	52
n_c	7	7	7	7	7	7	7	7
n in $\{vH\}^n$	2	2	2	2	2	2	2	2
$sd(p)$ (dB)	1.69	1.71	1.64	1.74	1.67	1.94	2.00	1.98
$sd(v)$ (m s^{-1})	1.49	1.52	1.48	1.54	1.52	1.58	1.47	1.53
$sd(w)$ (m s^{-1})	0.98	1.68	1.58	1.07	1.64	1.67	2.57	2.57
loss (%)	3.61%	13.3%	7.80%	5.49%	14.4%	7.28%	22%	14.2%
CSR (dB)	50	50	50	50	50	50	50	50
M^*	46	52	58	44	52	42	50	52
n_c	9	7	9	9	7	9	7	7
n in $\{vH\}^n$	2	2	2	2	2	2	2	2
$sd(p)$ (dB)	1.87	2.37	2.07	1.98	2.46	2.36	2.84	2.58
$sd(v)$ (m s^{-1})	1.61	1.02	1.33	1.57	1.03	1.51	0.83	1.07
$sd(w)$ (m s^{-1})	1.38	1.80	2.10	1.49	1.72	2.16	2.17	2.47
loss (%)	36.2%	62.7%	62.2%	48.1%	61.9%	54.7%	68.9%	61.9%

Note: M^* is the extended time series length. *loss* is the number of times the velocity is not resolved correctly as a percentage of the total number of simulations (about 2000). *loss* < 2% is generally observed to be because of the velocity folding at the ends of the Nyquist interval, $\pm v_a$. The n_c and n, the exponent of $\{\text{von Hann}\}^n$ is the optimum for the CSR (and the clutter width, w_c=0.28 m s^{-1}). The shaded part is for CSR=40dB, and the unshaded last 8 rows are for CSR=50 dB.

Table. 7.5a. Performance of the staggered PRT overlay algorithm for different elevation scans.

elv. deg.	T_u ms	*M**	v_a m s^{-1}	r_{a2} km	p_2/p_1 dB	w_1 m s^{-1}	w_2	$sd(p_1)$ dB	$sd(p_2)$ dB	$sd(v_1)$ m s^{-1}	$sd(v_2)$ m s^{-1}	$sd(w_1)$ m s^{-1}	$sd(w_2)$ m s^{-1}	$loss_1$ %	$loss_2$ %
2.40	0.61	40	45.08	274.5	0.0	3	3	1.28	1.24	0.93	0.91	0.51	0.49	0.00	0.05
2.40	0.61	40	45.08	274.5	3.0	3	3	1.26	1.24	0.99	0.96	0.52	0.52	0.05	0.00
2.40	0.61	40	45.08	274.5	6.0	3	3	1.25	1.26	0.94	0.94	0.51	0.67	0.15	0.00
2.40	0.61	40	45.08	274.5	9.0	3	3	1.26	1.26	0.95	1.02	0.51	0.86	0.15	0.00
2.40	0.61	40	45.08	274.5	12.0	3	3	1.27	1.24	0.89	0.97	0.49	0.78	0.25	0.05
2.40	0.61	40	45.08	274.5	15.0	3	3	1.29	1.23	0.91	0.94	0.51	0.66	0.59	0.00
2.40	0.61	40	45.08	274.5	18.0	3	3	1.26	1.23	0.91	0.87	0.50	0.57	1.93	0.00
2.40	0.61	40	45.08	274.5	21.0	3	3	1.23	1.23	0.93	0.85	0.49	0.54	2.38	0.00
2.40	0.61	40	45.08	274.5	24.0	3	3	1.26	1.25	0.92	0.86	0.51	0.51	4.50	0.00
2.40	0.61	40	45.08	274.5	27.0	3	3	1.25	1.30	0.95	0.86	0.51	0.51	8.02	0.00
2.40	0.61	40	45.08	274.5	30.0	3	3	1.25	1.24	0.97	0.85	0.48	0.49	9.55	0.00
3.35	0.55	40	50.00	247.5	0.0	3	3	1.31	1.32	0.90	0.90	0.52	0.53	0.00	0.05
3.35	0.55	40	50.00	247.5	4.0	3	3	1.31	1.25	0.90	0.89	0.53	0.54	0.05	0.00
3.35	0.55	40	50.00	247.5	8.0	3	3	1.34	1.32	0.87	1.01	0.51	0.96	0.05	0.00
3.35	0.55	40	50.00	247.5	12.0	3	3	1.30	1.32	0.91	1.02	0.53	0.85	0.00	0.00
3.35	0.55	40	50.00	247.5	16.0	3	3	1.33	1.34	0.87	0.94	0.52	0.69	0.10	0.00
3.35	0.55	40	50.00	247.5	20.0	3	3	1.33	1.30	0.97	0.88	0.52	0.58	0.50	0.00
3.35	0.55	40	50.00	247.5	24.0	3	3	1.31	1.32	0.92	0.87	0.50	0.53	0.79	0.00
3.35	0.55	40	50.00	247.5	28.0	3	3	1.32	1.33	0.88	0.87	0.53	0.53	1.39	0.00
3.35	0.55	40	50.00	247.5	32.0	3	3	1.30	1.31	0.88	0.88	0.53	0.52	2.82	0.00
3.35	0.55	40	50.00	247.5	36.0	3	3	1.33	1.32	0.89	0.88	0.52	0.52	5.69	0.00
3.35	0.55	40	50.00	247.5	40.0	3	3	1.28	1.32	0.91	0.88	0.52	0.51	9.90	0.00
4.30	0.46	52	59.78	207.0	0.0	3	3	1.31	1.29	0.84	0.82	0.51	0.51	0.00	0.00
4.30	0.46	52	59.78	207.0	5.0	3	3	1.25	1.28	0.83	0.88	0.50	0.64	0.00	0.00
4.30	0.46	52	59.78	207.0	10.0	3	3	1.30	1.28	0.85	1.06	0.50	1.20	0.00	0.00
4.30	0.46	52	59.78	207.0	15.0	3	3	1.29	1.32	0.85	0.94	0.50	0.85	0.00	0.00
4.30	0.46	52	59.78	207.0	20.0	3	3	1.28	1.27	0.82	0.87	0.50	0.59	0.00	0.00
4.30	0.46	52	59.78	207.0	25.0	3	3	1.28	1.29	0.83	0.84	0.51	0.52	0.00	0.00
4.30	0.46	52	59.78	207.0	30.0	3	3	1.29	1.28	0.85	0.82	0.50	0.51	0.00	0.00
4.30	0.46	52	59.78	207.0	35.0	3	3	1.25	1.26	0.85	0.84	0.50	0.50	0.00	0.00
4.30	0.46	52	59.78	207.0	40.0	3	3	1.27	1.25	0.85	0.86	0.50	0.49	0.05	0.00
4.30	0.46	52	59.78	207.0	45.0	3	3	1.26	1.28	0.85	0.83	0.50	0.51	0.54	0.00
4.30	0.46	52	59.78	207.0	50.0	3	3	1.26	1.30	0.82	0.87	0.51	0.51	4.11	0.00

Table. 7.5b. Performance of the staggered PRT overlay algorithm for different elevation scans.

elv. deg.	T_u ms	*M**	v_a m s^{-1}	r_{a2} km	p_2/p_1 dB	w_1	w_2 m s^{-1}	$sd(p_1)$ dB	$sd(p_2)$ dB	$sd(v_1)$	$sd(v_2)$ m s^{-1}	$sd(w_1)$	$sd(w_2)$ m s^{-1}	$loss_1$ %	$loss_2$ %
2.40	0.61	40	45.08	274.5	0.0	4	4	1.07	1.09	2.15	1.99	0.60	0.57	2.33	1.98
2.40	0.61	40	45.08	274.5	2.0	4	4	1.09	1.10	1.92	2.05	0.57	0.58	2.57	1.44
2.40	0.61	40	45.08	274.5	4.0	4	4	1.12	1.08	1.94	2.04	0.59	0.59	3.07	1.24
2.40	0.61	40	45.08	274.5	6.0	4	4	1.08	1.09	2.04	2.03	0.58	0.67	5.35	0.79
2.40	0.61	40	45.08	274.5	8.0	4	4	1.12	1.13	1.98	1.82	0.58	0.83	9.06	0.74
2.40	0.61	40	45.08	274.5	10.0	4	4	1.09	1.12	2.00	1.42	0.59	0.82	11.83	0.05
2.40	0.61	40	45.08	274.5	12.0	4	4	1.11	1.09	1.92	1.11	0.58	0.80	17.87	0.00
2.40	0.61	40	45.08	274.5	14.0	4	4	1.08	1.13	1.87	1.07	0.58	0.76	21.63	0.00
2.40	0.61	40	45.08	274.5	16.0	4	4	1.10	1.10	1.88	1.01	0.60	0.69	23.56	0.00
2.40	0.61	40	45.08	274.5	18.0	4	4	1.12	1.09	1.90	1.00	0.58	0.67	29.80	0.00
2.40	0.61	40	45.08	274.5	20.0	4	4	1.12	1.09	1.93	0.96	0.58	0.65	37.62	0.00
3.35	0.55	40	50.00	247.5	0.0	4	4	1.17	1.15	1.72	1.64	0.64	0.63	0.69	0.54
3.35	0.55	40	50.00	247.5	2.0	4	4	1.16	1.15	1.59	1.72	0.64	0.65	0.79	0.89
3.35	0.55	40	50.00	247.5	4.0	4	4	1.17	1.16	1.65	1.68	0.65	0.63	1.14	0.74
3.35	0.55	40	50.00	247.5	6.0	4	4	1.17	1.17	1.56	1.57	0.63	0.76	2.03	0.69
3.35	0.55	40	50.00	247.5	8.0	4	4	1.14	1.14	1.58	1.63	0.65	0.91	2.82	0.25
3.35	0.55	40	50.00	247.5	10.0	4	4	1.11	1.16	1.58	1.34	0.64	0.94	4.46	0.30
3.35	0.55	40	50.00	247.5	12.0	4	4	1.19	1.17	1.55	1.20	0.61	0.83	6.34	0.00
3.35	0.55	40	50.00	247.5	14.0	4	4	1.14	1.16	1.61	1.10	0.63	0.78	9.16	0.00
3.35	0.55	40	50.00	247.5	16.0	4	4	1.16	1.15	1.50	1.12	0.63	0.73	11.53	0.00
3.35	0.55	40	50.00	247.5	18.0	4	4	1.13	1.15	1.53	1.06	0.62	0.69	15.10	0.00
3.35	0.55	40	50.00	247.5	20.0	4	4	1.15	1.11	1.65	1.02	0.63	0.68	18.86	0.00
4.30	0.46	52	59.78	207.0	0.0	4	4	1.14	1.10	1.12	1.20	0.64	0.66	0.20	0.15
4.30	0.46	52	59.78	207.0	3.0	4	4	1.10	1.12	1.14	1.17	0.65	0.65	0.35	0.30
4.30	0.46	52	59.78	207.0	6.0	4	4	1.08	1.09	1.19	1.11	0.66	0.84	0.30	0.35
4.30	0.46	52	59.78	207.0	9.0	4	4	1.10	1.11	1.17	1.25	0.64	1.11	0.25	0.15
4.30	0.46	52	59.78	207.0	12.0	4	4	1.12	1.13	1.16	1.14	0.65	0.96	0.35	0.00
4.30	0.46	52	59.78	207.0	15.0	4	4	1.11	1.11	1.18	1.07	0.68	0.79	0.64	0.00
4.30	0.46	52	59.78	207.0	18.0	4	4	1.13	1.10	1.05	1.01	0.63	0.71	0.94	0.00
4.30	0.46	52	59.78	207.0	21.0	4	4	1.12	1.10	1.11	0.98	0.66	0.63	1.53	0.00
4.30	0.46	52	59.78	207.0	24.0	4	4	1.12	1.12	1.22	0.97	0.69	0.61	3.27	0.00
4.30	0.46	52	59.78	207.0	27.0	4	4	1.10	1.07	1.10	1.01	0.63	0.60	5.40	0.00
4.30	0.46	52	59.78	207.0	30.0	4	4	1.10	1.12	1.16	0.98	0.68	0.60	7.13	0.00

10. References

1. Doviak, R. J. and D. S. Zrnic, **1993**: *Doppler Radar and Weather Observations.*, Academic Press, New York, 562 pp.
2. Charles L. Frush, **1999**: NEXRAD Range-Velocity: Exploring selected mitigation techniques, 2nd year report, NCAR, May 6,1999.
3. Evans, J., **2001**: Personal communication.
4. Sachidananda, M., D. S. Zrnic, and R. J. Doviak, **1997**: Signal design and processing techniques for WSR-88D ambiguity resolution, Part-1. *National Severe Storms Laboratory*, July 1997, 100 pp.
5. Sachidananda, M., D. S. Zrnic, and R. J. Doviak, **1998**: Signal design and processing techniques for WSR-88D ambiguity resolution, Part-2. *National Severe Storms Laboratory*, June 1998, 105 pp.
6. Sachidananda, M., D. S. Zrnic, and R. J. Doviak, **1999**: Signal design and processing techniques for WSR-88D ambiguity resolution, Part-3. *National Severe Storms Laboratory*, July 1999, 81 pp.
7. Sachidananda, M., D. S. Zrnic, and R. J. Doviak, **2000**: Signal design and processing techniques for WSR-88D ambiguity resolution, Part-4. *National Severe Storms Laboratory*, October 2000, 99 pp.
8. Sirmans, D, D. Zrnic, and B. Bumgarner, 1976: Extension of maximum unambiguous Doppler velocity by use of two sampling rates, *Preprints 17th Conference on Radar Meteorology*, Seattle, WA, AMS, pp 23-28.
9. Zrnic, D. S., and P. R. Mahapatra, **1985**: Two methods of ambiguity resolution in pulsed Doppler weather radars. *IEEE Trans. on Aerospace and Electronic Systems.*, vol. **AES-21,** 470-483.

LIST OF NSSL REPORTS FOCUSED ON
POSSIBLE UPGRADES TO THE WSR-88D RADARS.

1. Fang, M, and R. J. Doviak, **2001**: Spectrum width statistics of various weather phenomena, 64 pp.
2. Sachidananda, M., **2000:** Signal Design and Processing Techniques for WSR-88D Ambiguity Resolution, Part 4, 99 pp.
3. Sachidananda, M., **1999:** Signal Design and Processing Techniques for WSR-88D Ambiguity Resolution, Part 3, 81 pp.
4. Doviak, R. J. and D. S. Zrnic, **1998:** NOAA/NSSL's WSR-88D Radar for Research and Enhancement of Operations: Polarimetric Upgrades to Improve Rainfall Measurements, 110 pp.
5. Sachidananda, M., **1998:** Signal Design and Processing Techniques for WSR-88D Ambiguity Resolution, Part 2, 105 pp.
6. Sachidananda, M., **1997:** Signal Design and Processing Techniques for WSR-88D Ambiguity Resolution, Part 1, 100 pp.
7. Sirmans, D., D. S. Zrnic, and M. Sachidananda, **1986:** Doppler radar dual polarization considerations for NEXRAD, Part 1, 109 pp.
8. Sirmans, D., D. S. Zrnic, and N. Balakrishnan, **1986:** Doppler radar dual polarization considerations for NEXRAD, Part 2, 70 pp.